Spectroscopic study of the ^{64,66,68}Ni isotopes populated in ^{64}Ni + ^{238}U collisions

R. Broda,[1] T. Pawłat,[1] W. Królas,[1] R. V. F. Janssens,[2] S. Zhu,[2] W. B. Walters,[3] B. Fornal,[1] C. J. Chiara,[2,3] M. P. Carpenter,[2] N. Hoteling,[3] Ł. W. Iskra,[1] F. G. Kondev,[4] T. Lauritsen,[2] D. Seweryniak,[2] I. Stefanescu,[2,3] X. Wang,[2] and J. Wrzesiński[1]

[1]*The H. Niewodniczanski Institute of Nuclear Physics PAN, PL-31342 Kraków, Poland*

[2]*Physics Division, Argonne National Laboratory, Argonne, Illinois 60439, USA*

[3]*Department of Chemistry and Biochemistry, University of Maryland, College Park, Maryland 20742, USA*

[4]*Nuclear Engineering Division, Argonne National Laboratory, Argonne, Illinois 60439, USA*

(Received 5 October 2012; published 12 December 2012)

Excited states in ^{64}Ni, ^{66}Ni, and ^{68}Ni were populated in quasielastic and deep-inelastic reactions of a 430-MeV ^{64}Ni beam on a thick ^{238}U target. Level schemes including many nonyrast states were established up to respective excitation energies of 6.8, 8.2, and 7.8 MeV on the basis of γ-ray coincidence events measured with the Gammasphere array. Spin-parity assignments were deduced from an angular-correlation analysis and from observed γ-decay patterns, but information from earlier γ-spectroscopy and nuclear-reaction studies was used as well. The spin assignments for nonyrast states were supported further by their observed population pattern in quasielastic reactions selected through a cross-coincidence technique. Previously established isomeric-state decays in ^{66}Ni and ^{68}Ni were verified and delineated more extensively through a delayed-coincidence analysis. A number of new states located above these long-lived states were identified. Shell-model calculations were carried out in the $p_{3/2}f_{5/2}p_{1/2}g_{9/2}$ model space with two effective interactions using a ^{56}Ni core. Satisfactory agreement between experimental and computed level energies was achieved, even though the calculations indicate that all the states are associated with rather complex configurations. This complexity is illustrated through the discussion of the structure of the negative-parity states and of the *M1* decays between them. The best agreement between data and calculations was achieved for ^{68}Ni, the nucleus where the calculated states have the simplest structure. In this nucleus, the existence of two low-spin states reported recently was confirmed as well. Results of the present study do not indicate any involvement of collective degrees of freedom and confirm the validity of a shell-model description in terms of neutron excitations combined with a closed $Z = 28$ proton shell. Further improvements to the calculations are desirable.

DOI: 10.1103/PhysRevC.86.064312 PACS number(s): 23.20.Lv, 21.60.Cs, 27.50.+e, 25.70.Lm

I. INTRODUCTION

Rapid changes in structure observed as a function of the proton-to-neutron ratio of the nuclear system have recently attracted strong interest and motivated extensive studies of neutron-rich nuclei in the Ni region. An important aspect of such investigations focuses on the presence of shell gaps for specific "magic" numbers of nucleons as the latter represent cornerstones of nuclear structure. Over the past decade, it has become increasingly clear that these magic numbers are not immutable and depend on the proton-to-neutron composition of nuclei [1,2]. In the case of the Ni isotopic chain, the closed $Z = 28$ proton shell stabilizes a spherical shape near the ground state in a long series of nuclei. Consequently, their level structure at low and moderate spin is expected to be described well within the framework of the shell model. In this series of isotopes, the doubly magic nuclei, for example, the $N = Z = 28$ nucleus ^{56}Ni and the neutron-rich $N = 50$ ^{78}Ni, define the mass range where the filling of the $p_{3/2}$, $f_{5/2}$, $p_{1/2}$, and $g_{9/2}$ neutron orbitals primarily determines the structure of low-energy excitations. In the middle of this range, the $N = 40$ subshell closure was established in ^{68}Ni by the observation of a 1770-keV, 0_2^+ lowest excited state [3] and the subsequent identification of a high-energy 2034-keV, 2_1^+ level, as well as of a long-lived 5^- isomer [4]. The $N = 40$ energy gap separating the $p_{1/2}$ and $g_{9/2}$ single-particle levels is estimated to be of the order of only 2 MeV. However, the gap seems to persist in heavier Ni isotopes where the anticipated $g_{9/2}$ seniority isomers in ^{69}Ni and ^{70}Ni have been identified [5]. Furthermore, the addition of one proton does not appear to affect the $N = 40$ subshell closure much: In the neighboring ^{69}Cu and ^{71}Cu isotopes, "shell-model" isomers have also been observed [6–8]. Moreover, the high excitation energy of the first yrast transition identified above the ^{71}Cu isomer mirrors closely that of the 2^+ excitation in the ^{68}Ni core [9].

The situation is drastically different for nuclei with a proton number lower than $Z = 28$. β-decay studies [10–13] as well as in-beam investigations with intermediate-energy fragments [14–17] provide evidence for the onset of collectivity in neighboring nuclei of the Ni region. Specifically, the 2^+ levels of $N = 40$, ^{64}Cr [15] and ^{66}Fe [10], are located at excitation energies as low as 420 and 573 keV, respectively, indicating a strong polarization of the ^{68}Ni core and a presence of deformed components in the wave functions of low-spin states. It is by now well established that the strongly attractive monopole tensor force between the $f_{7/2}$ protons and $f_{5/2}$ neutrons, which is primarily responsible for the appearance of the neutron $f_{5/2}$–$g_{9/2}$ energy gap, becomes less effective when successive $f_{7/2}$ protons are removed from the closed $Z = 28$ shell [1,2]. With a diminishing subshell gap, the occupation of the high-j, $g_{9/2}$ neutron orbital increases and drives nuclear deformation effects.

A satisfactory description of nuclear structure in this Ni region is still lacking and, therefore, additional efforts are required to obtain new experimental information and/or to

solidify previously established level schemes. As stated above, the neutron-rich Ni isotopes are of particular importance because they involve, at low and moderate spin, structures arising predominantly from neutron excitations which, up to rather high excitation energies, are largely unaffected by protons strongly bound in the closed $Z = 28$ shell. Recently, the present collaboration has published results of a spectroscopic study of the ^{67}Ni isotope [18]. In the present work, a new detailed study of ^{64}Ni and ^{66}Ni is presented which completes and, in many instances, amplifies the previously available experimental information on these nuclei. The ^{68}Ni isotope is included in the present investigation as well, and the level scheme established earlier [4], [6] has been extended to higher spin states. In addition, comparisons with shell-model calculations incorporating recently proposed effective interactions are discussed.

The most recent spectroscopic study of the ^{64}Ni and ^{66}Ni isotopes [19] was performed in the early stages of the application of deep-inelastic heavy-ion collisions to the spectroscopy of neutron-rich nuclei [20]. Use was made of the ^{64}Ni + ^{208}Pb reaction to carry out a γ-γ coincidence measurement with the 12-detector OSIRIS spectrometer, a rather modest array by present-day standards. Here, extensive data were obtained with the ^{64}Ni + ^{238}U reaction and the powerful Gammasphere γ-detector array. Whereas this experiment did already provide results on a few other nuclei in the region [21–23], the primary aim of the present effort was to analyze γ-γ angular correlations to verify earlier tentative spin-parity assignments of levels observed in the ^{64}Ni and ^{66}Ni isotopes. However, the new data revealed more detailed information on both level schemes, including on a number of weakly populated nonyrast states. In some instances, the new findings could be confronted with earlier information on these levels compiled from various studies in Refs. [24,25]. It is quite likely that the presently established level schemes include most, if not all, the information on ^{64}Ni and ^{66}Ni that can be extracted through modern deep-inelastic heavy-ion spectroscopy with a thick target. In the case of the ^{68}Ni isotope, an experiment with a ^{70}Zn beam may, possibly, provide still better data on hitherto unknown nonyrast states.

II. EXPERIMENTAL DETAILS AND ANALYSIS

The experiment was carried out with a 430-MeV ^{64}Ni beam delivered by the ATLAS superconducting linear accelerator facility at Argonne National Laboratory. The isotopically enriched ^{238}U target with a 55 mg/cm^2 thickness was located at the center of the Gammasphere array [26], consisting of 100 Compton-suppressed high-purity germanium (HPGe) detectors for this measurement. The target thickness was sufficient to stop all reaction products arising in binary processes taking place at collision energies ranging from the initial 430-MeV down to below the Coulomb barrier. The ^{64,66,68}Ni nuclei investigated here were populated through a number of different quasielastic and deep-inelastic processes taking place within this energy range in collisions between ^{64}Ni ions and ^{238}U target nuclei. The emitted γ rays were detected by the Gammasphere array with the requirement that three or more Compton-suppressed detectors fire in coincidence. For a small part (20%) of the measurement, the event trigger condition was relaxed to allow twofold coincidence events to be recorded as well. The beam was pulsed with a 412-ns repetition rate, each beam pulse being ∼0.3 ns wide. A total of 2.5×10^9 events satisfying the fold three trigger or greater trigger condition was recorded. It is worth noting that for some part of the analysis, use was also made of the data from a similar experiment performed with the 330-MeV ^{48}Ca + ^{238}U reaction for which the relevant details are described elsewhere [20].

The collected γ-coincidence data were sorted into two-dimensional (E_γ-E_γ matrices) and three-dimensional (E_γ-E_γ-E_γ cubes) histograms under various timing conditions. In the main part of the analysis, prompt events (PP or PPP histograms) were inspected by placing a coincidence time window within ±20 ns of the beam burst. Only in the case of the ^{66}Ni isotope did the presence of a short-lived (4.3 ns) isomer require a dedicated sort of the data with time parameters selecting an appropriate delayed range which clarified the isomer location (see discussion below). To investigate coincidence relationships below or across an isomer, delayed-delayed (DD,DDD) and prompt-delayed (PD,PDD) histograms were created as well. Here, the prompt (P) condition was defined as indicated above and the delayed (D) time ranges of 8–45 ns and 10–150 ns were selected for the analysis of the ^{66}Ni and ^{68}Ni isomers, respectively. In a standard delayed cube (DDD), the transitions were required to occur in an interval ∼40 to ∼800 ns after the prompt time peak (excluding the subsequent beam pulse), but within ∼20 ns of each other. For Ni isotopes, this cube involved predominantly events arising from β decays of the corresponding Co isotopes.

From the analysis of threefold coincidences, detailed level schemes for ^{64}Ni and ^{66}Ni were established and firm placement was provided for all γ transitions with intensities down to a detection limit of 0.2% of the channel strength. For this quantitative analysis, the intensities of the transitions feeding the first 2^+ states were determined from the coincidence data collected with the fold two trigger condition. The present study was primarily focused on ^{64}Ni and ^{66}Ni nuclei. The analysis concerning the ^{68}Ni isotope is described in a separate short section.

The inspection of the delayed coincidence events between the beam pulses also revealed the population of ^{64}Ni and ^{66}Ni levels in β decay of the ^{64}Co and ^{66}Co isotopes, respectively. Whereas in the ^{64}Co decay few previously unknown branches could be established, these observations are only briefly addressed below in the discussion of the ^{64}Ni level scheme because a collaboration at ISOLDE has recently obtained more complete information from a dedicated study of this decay [27].

An essential aspect of the present analysis was focused on the determination of angular-correlation coefficients to provide spin-parity assignments to the observed levels. For this purpose, the double coincidence data were sorted into four matrices corresponding to the 19°, 45°, 69°, and 85° average angles between Gammasphere detectors. Although the detector pairs in the array could be divided into more precise angle definitions resulting in additional experimental data points, this would be done at the expense of statistical

accuracy and the present division into four angles was found to be optimal for the weaker transitions as it enabled a consistent extraction of peak areas from the coincidence spectra with a controlled background. The resulting intensities were properly normalized to the number of detector pairs at each angle and fitted using the standard Legendre-polynomial expression $W(\theta) = a_o[1 + a_2 P_2(\cos\theta) + a_4 P_4(\cos\theta)]$ to extract a_2 and a_4 coefficients. For the most typical cases, the expected values of the angular correlation coefficients are $a_2 = 0.10$ and $a_4 = 0.01$ for a pure quadrupole-quadrupole cascade, $a_2 = -0.07$ and $a_4 = 0.0$ for a pure quadrupole-dipole sequence, and finally $a_2 = 0.05$ and $a_4 = 0.0$ for a pure dipole-dipole case [28].

III. RESULTS: LEVEL SCHEMES AND SPIN-PARITY ASSIGNMENTS

A. ^{64}Ni

The present study confirmed the ^{64}Ni level scheme established earlier [19] and extended it by a few transitions in the high-spin and excitation energy regions. Most of the new results concern previously unobserved weak transitions and herewith substantially clarify information on nonyrast states. It is important to realize that the excited states of the ^{64}Ni projectile nucleus observed in this work are populated through several different types of reactions which take place in ^{64}Ni + ^{238}U collisions at beam energies ranging, in the thick target, from the initial 430 MeV down to well below the Coulomb barrier. Peripheral collisions involving Coulomb excitation and inelastic nuclear scattering predominantly populate low-spin states. These nonyrast ^{64}Ni excitations are accompanied by an intense population of the ground-state band and other states in the ^{238}U target nucleus. Higher-spin ^{64}Ni yrast states are fed in more violent nuclear processes, which often involve neutron transfer followed by subsequent neutron evaporation. These features can be seen readily in Fig. 1, which displays the low-energy part of the γ coincidence spectrum

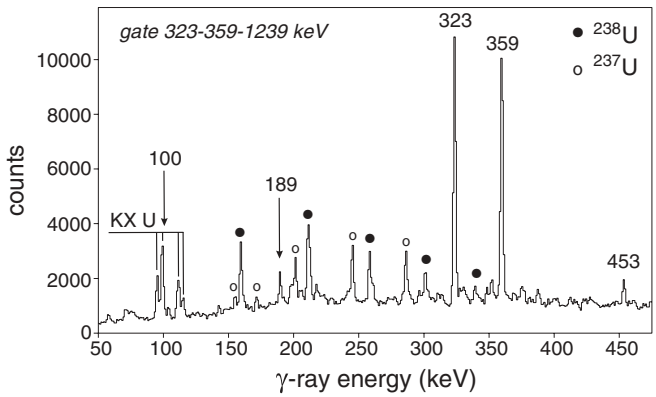

FIG. 1. Low-energy part of the coincidence spectrum with double gates placed on all pairs of 323-, 359-, and 1239-keV yrast transitions in ^{64}Ni. Lines in ^{64}Ni are marked by energies and γ rays in ^{238}U and ^{237}U, resulting from the cross-coincidence between transitions in projectilelike and targetlike nuclei, are indicated by solid and open circles, respectively.

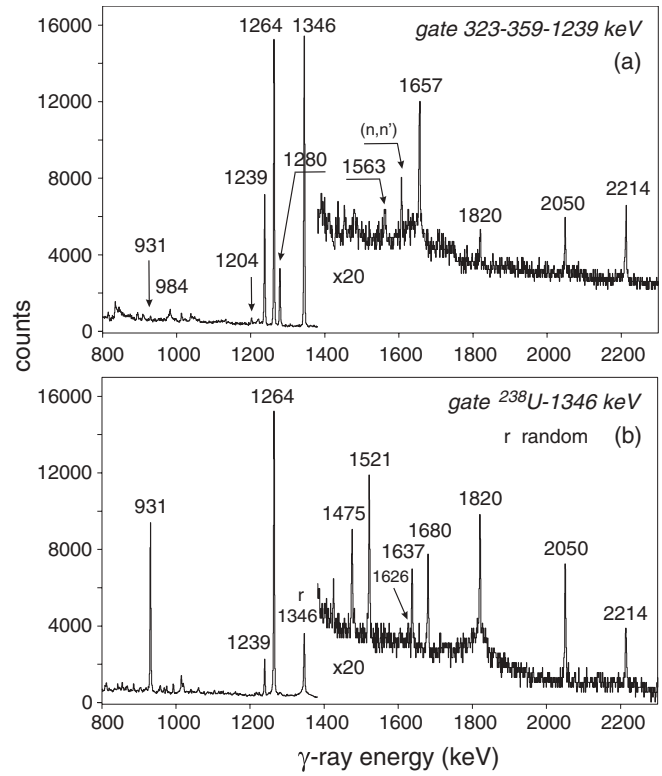

FIG. 2. High-energy parts of double-gated coincidence spectra enhancing the observation of yrast (a) and nonyrast (b) transitions in ^{64}Ni. Spectrum (a) is the high-energy part of the spectrum displayed in Fig. 1. Spectrum (b) was obtained with coincidence gates placed on the 1346-keV, $2_1^+ \rightarrow 0^+$ ground-state transition and any γ line from the ^{238}U ground-state band up to the 14^+ level (see text for details).

obtained with double gates placed on all combinations of the 323-, 359-, and 1239-keV yrast transitions in ^{64}Ni. In this energy range, apart from the four ^{64}Ni transitions marked by their respective energies, a series of lines corresponding to the ground-state bands of the ^{238}U and ^{237}U isotopes is clearly visible, as indicated by solid and open dots, respectively. Closer inspection of this spectrum also demonstrates the presence of the ^{236}U isotope where the corresponding γ rays appear as the high-energy components of ^{238}U lines because of the closeness in the nominal transition energies. Moreover, the low intensity of these uranium cross-coincidence transitions relative to the main ^{64}Ni γ rays indicates that the yrast states in the ^{64}Ni nucleus of interest are also populated by even more violent processes involving fission of the target.

Figure 2(a) displays the high-energy part of the same coincidence spectrum of Fig. 1. Here, the lines of ^{64}Ni indicated in the figure include intense known transitions in the main yrast sequence [19] as well as the 984-, 1204-, 1563-, and 1657-keV new, weak γ rays located in the upper part of the level scheme. The marked high-energy 1820-, 2050-, and 2214-keV lines represent low-lying transitions which are populated by competing deexcitation branches, parallel to the 1239-keV γ ray, below the 323- and 359-keV transition pair involved in the gating condition. The spectrum displayed in the same energy range in Fig. 2(b) was obtained by summing coincidence spectra with double gates set on the 1346-keV,

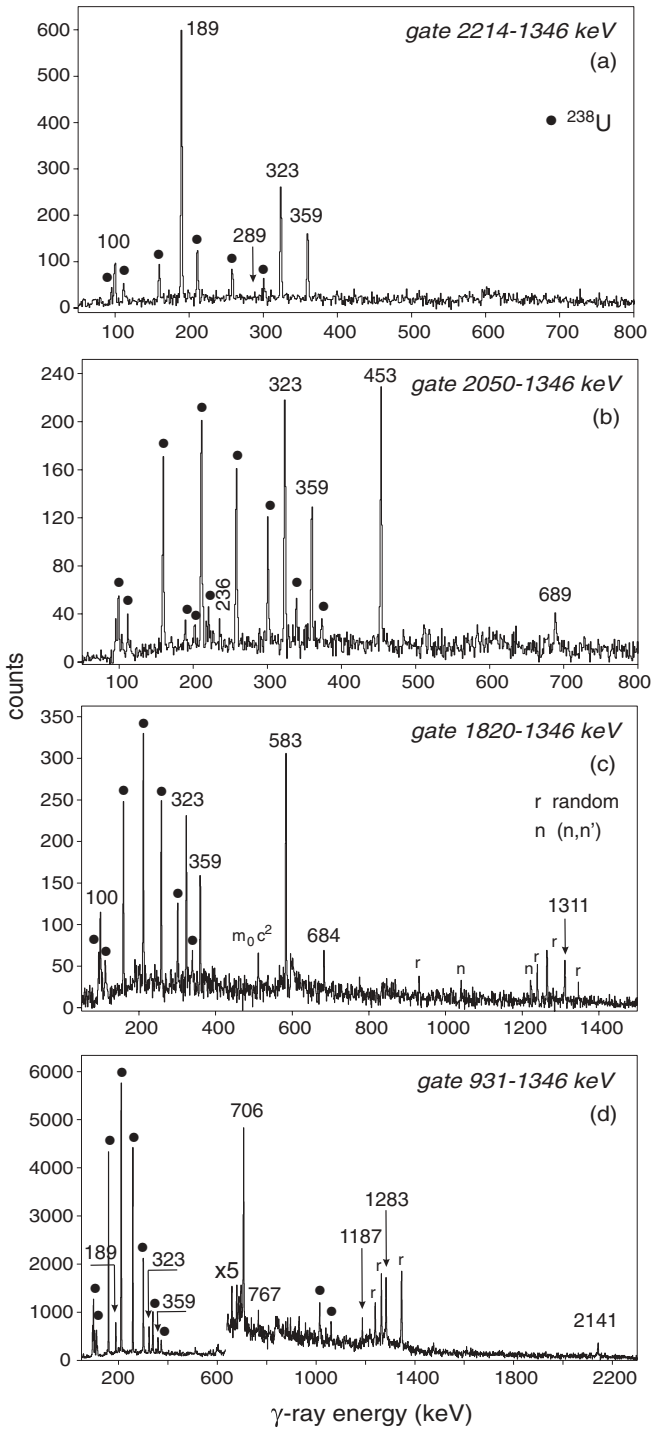

FIG. 3. Selected examples of ^{64}Ni coincidence spectra with double gates placed on the 1346-keV, $2_1^+ \rightarrow 0^+$ transition and γ rays feeding the 2_1^+ level as indicated in each panel. The cross-coincidence transitions from ^{238}U are marked by solid points and the background lines arising from random coincidences and accompanying (n,n') γ rays are marked with r and n labels, respectively.

^{64}Ni $2^+ \rightarrow 0^+$ transition together with any of the ^{238}U ground-state-band transitions. A comparison of Figs. 2(a) and 2(b) indicates a noticeable difference in yrast and nonyrast populations in ^{64}Ni. The selection of events requiring the presence of the excited ^{238}U isotope [Fig. 2(b)] served to identify all transitions feeding the lowest 2^+ state in ^{64}Ni with an intensity larger than the 0.2% detection limit.

Examples of coincidence spectra displayed in Fig. 3 demonstrate the quality of the data by highlighting weak decay branches populating selected nonyrast levels from higher-lying states. The high intensity of the ^{238}U transitions in these spectra, as compared to Fig. 1, is a function of the selected coincidence gates and reemphasizes the sizeable population of these specific nonyrast ^{64}Ni states.

The complete scheme, including all ^{64}Ni levels observed in the present work, is displayed in Fig. 4 and the relevant numerical data on γ-transition energies and intensities are listed in Table I. Results from the angular-correlation analysis are included as well for all transitions for which meaningful a_2 and a_4 coefficients could be obtained with coincidence gates placed on transitions of known multipolarity. The latter are given in the last column of Table I. Examples of $W(\theta)$ distributions and fitting results, representative of transitions in ^{64}Ni, are displayed in Fig. 5.

Whereas angular-correlation results provided the main basis for spin-parity assignments, additional information on spin values was obtained from a quantitative comparison of the populations of ^{64}Ni yrast and nonyrast states. In Table II, ratios of intensities are given between the strength of each transition deexciting a given state in quasielastic processes (I_Q) and that derived from the total population of this level ($I_{\rm TOT}$) through all possible reactions. These ratios were formed by using the corresponding peak areas in the coincidence spectrum obtained from all combinations of double gates placed on the ^{238}U ground-state band transitions (I_Q) and in a similar spectrum with a single gate on the 1346-keV, $2^+ \rightarrow 0^+$^{64}Ni transition ($I_{\rm TOT}$). As discussed above, selecting events in which ^{238}U excitations accompany ^{64}Ni transitions in the reaction exit channel strongly favors the population of nonyrast states. The ratios in Table II, normalized to unity for the 1264-keV $4^+ \rightarrow 2^+$ transition, show clearly the reduction in yrast-state population and a general enhancement in nonyrast transition intensities in quasielastic reactions. For comparison, similar ratios were formed to demonstrate the enhancement of yrast-state population in ^{64}Ni when the latter nucleus is produced in the 330-MeV ^{48}Ca + ^{238}U reaction. As mentioned above, the data obtained in an earlier experiment with a ^{48}Ca beam revealed a sizable Ni production yield resulting from massive nucleon-transfer reactions with subsequent evaporation of up to 12 neutrons. Indeed, the ratios listed in Table II of the corresponding transition intensities, observed in coincidence with the 1346-keV ^{64}Ni transition, exhibit a drastic increase in yrast-state population and a strong reduction in the population of nonyrast states for the U + Ca system.

In the following, some details of the level scheme are discussed together with the spin-parity assignments that are proposed for most of the reported levels (Fig. 4). Starting from the well-established 4^+ level at 2610 keV, the angular-correlation results (Table I) involving the 1239-, 323-, 359-, and 1280-keV prominent yrast transitions establish uniquely the respective 5^-, 6^-, 7^-, and 8^+ assignments to the 3849-, 4172-, 4532-, and 5812-keV levels, in agreement with the earlier suggestion of Ref. [19]. It is worth noting that the

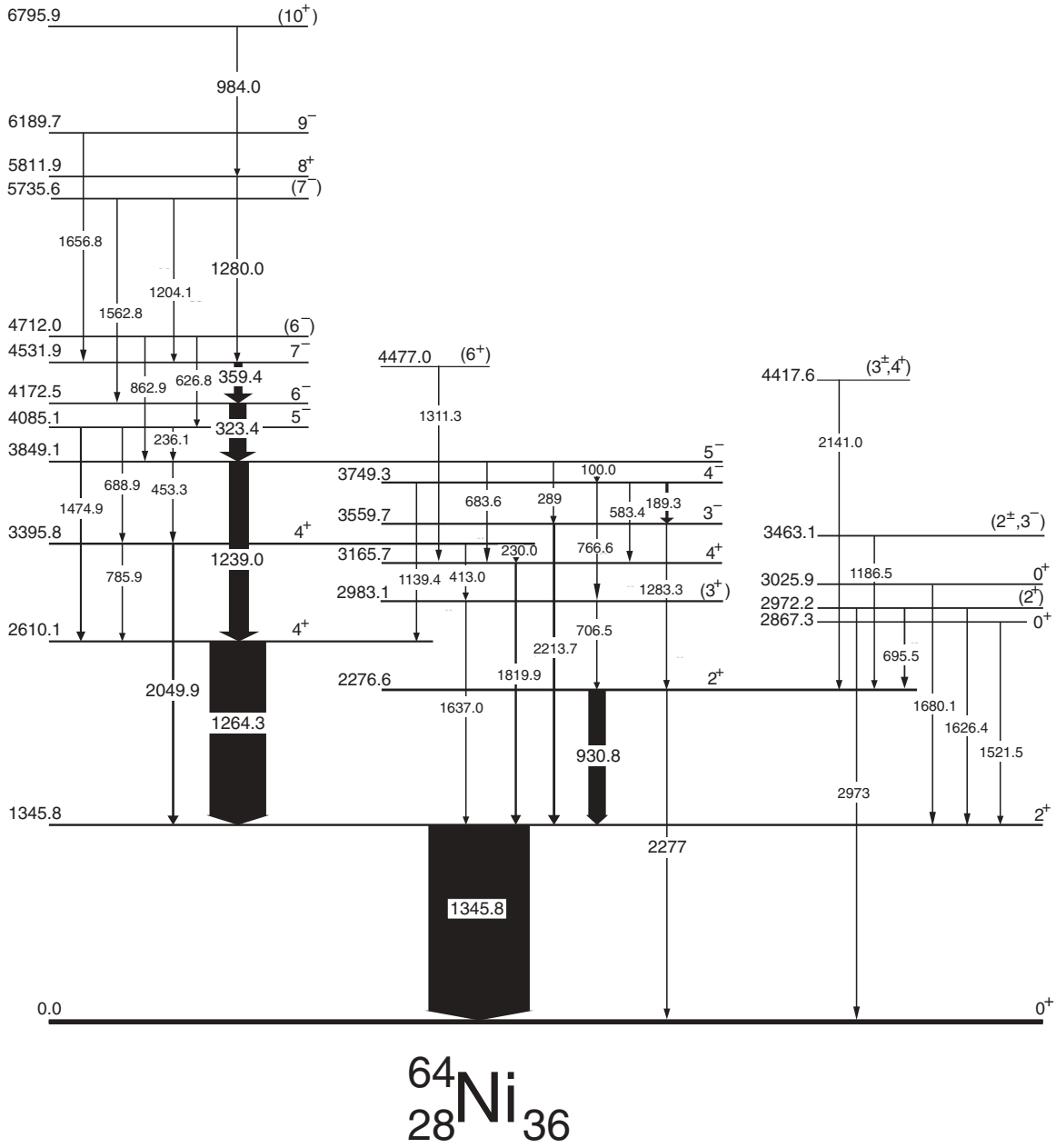

FIG. 4. ^{64}Ni level scheme established in the present study. The widths of the arrows reflect the observed transition intensities for the strongest transitions only. The spin-parity assignments are discussed in detail in the text.

proposed increase in spin with excitation energy is now confirmed by the quantitative yrast-population results of Table II. In the upper part of the level scheme, the 430-keV transition located previously [19] was not observed, but three new levels were established at 5736, 6190, and 6796 keV. Of those, only the 6190-keV level could be uniquely assigned as a 9^- state, but the two weak transitions of 1204 and 1563 keV to the lower-lying 7^- and 6^- levels favor a tentative 7^- assignment for the 5736-keV nonyrast state. The tentative 10^+ assignment to the 6796-keV level is based on the observed selective decay via the 984-keV transition to the 8^+ state and on the likely yrast nature of this state, the highest-energy one located in the present study. In the lower part of the scheme, the 4085-keV nonyrast state, for which no feeding from levels above could be detected, was established as the 5^-_2 level based on the angular-correlation result extracted for the main 1475-keV decay transition (Table I). In this part, yet another weakly populated nonyrast level was established at 4712 keV and assigned tentatively as the 6^- state on the basis of its exclusive decay to the two lower-lying 5^- states.

The 2277-keV level was uniquely assigned as the second 2^+ state in agreement with the previous tentative assignment [24]. As expected, this state is populated in the ^{64}Co, 1^+ ground-state β decay and the accurate angular-correlation coefficients measured here characterize the intense 931-keV γ-ray depopulating this state to the 2^+_1 level as a $\Delta I = 0$, $M1/E2$ mixed

TABLE I. List of levels identified in ^{64}Ni with their respective spin-parity assignments and the properties of the depopulating transitions. The reported intensities are normalized to the total feeding of the 1345.8-keV, 2_1^+ state (defined as 100). Measured angular-correlation coefficients together with the respective gating transitions are given in the last three columns. For some transitions, results involving several gating transitions are presented. Gating transitions with multipolarities other than *E2* are marked with a * sign.

E_{level} (keV)	I^π	E_γ (keV)	I_γ (rel.)	a_2	a_4	Gate
1345.8	2^+	1345.8(1)	100			
2276.6	2^+	930.8(1)	21.5(5)	−0.25(3)	0.15(4)	1346
		2277(2)	0.18(5)			
2610.1	4^+	1264.3(1)	65.0(5)	0.08(1)	0.03(2)	1346
2867.3	0^+	1521.5(2)	1.3(2)	0.43(15)	0.75(20)	1346
2972.2	(2^+)	695.5(3)	0.4(2)			
		1626.4(4)	0.5(3)			
		2973(1)	0.4(2)			
2983.1	(3^+)	706.5(2)	2.5(3)	0.07(6)		1346
		1637.0(3)	1.6(3)	0.06(6)	−0.02(11)	1346
3025.9	0^+	1680.1(2)	0.6(2)	0.60(20)	0.80(20)	1346
3165.7	4^+	1819.9(2)	3.2(4)	0.10(6)	–	1346
3395.8	4^+	230.0(3)	0.18(8)			
		413.0(3)	0.20(5)			
		785.9(2)	1.6(3)	0.19(6)	−0.03(6)	1264
		2049.9(2)	2.7(4)	0.13(6)	0.04(10)	1346
3463.1	$(2^\pm,3^-)$	1186.5(3)	0.3(1)			
3559.7	3^-	1283.3(3)	0.9(2)			
		2213.7(2)	3.2(4)	−0.07(4)	−0.02(4)	1346
3749.3	4^-	189.3(3)	3.3(3)	−0.05(4)	–	1346
		583.4(3)	1.2(2)	0.24(8)	–	1820
		766.6(4)	0.25(5)			
		1139.4(3)	0.6(2)			
3849.1	5^-	100.0(3)	1.1(3)			
		289(1)	0.12(7)			
		453.3(3)	1.4(3)	−0.17(10)	0.02(10)	2050
		683.6(4)	0.2(1)			
		1239.0(1)	23.0(2)	−0.08(2)	0.02(3)	1264
				−0.08(1)	0.03(1)	1346
4085.1	5^-	236.1(3)	0.7(3)			
		688.9(3)	0.20(5)			
		1474.9(3)	2.1(3)	−0.07(3)	0.03(4)	1264
				−0.08(5)	0.01(10)	1346
4172.5	6^-	323.4(1)	20.1(2)	−0.06(3)	0.04(5)	1346
				−0.05(1)	0.04(3)	1264
4417.6	$(3^\pm,4^+)$	2141.0(3)	0.4(1)			
4477.0	(6^+)	1311.3(4)	0.25(5)			
4531.9	7^-	359.4(1)	12.0(2)	−0.08(2)	0.00(3)	1264
				0.04(1)	0.01(2)	323*
				−0.06(2)	0.03(3)	1346
4712.0	(6^-)	626.8(3)	0.3(2)			
		862.9(2)	1.1(2)			
5735.6	(7^-)	1204.1(3)	0.5(2)			
		1562.8(4)	0.4(2)			
5811.9	8^+	1280.0(2)	1.9(3)	0.04(1)	0.07(6)	359*
				−0.10(8)	−0.04(10)	1264
6189.7	9^-	1656.8(3)	0.5(2)	0.11(3)	0.01(4)	1264
6795.9	(10^+)	984.0(4)	0.3(1)			

transition with a mixing ratio $\delta \sim -0.9$. With this mixing, the calculated a_2 and a_4 coefficients for the $2_2^+ \rightarrow 2_1^+ \rightarrow 0^+$ sequence are -0.26 and $+0.15$, in good agreement with the experimental values, whereas another solution, satisfying the measured a_2 value, would require the 931-keV transition to be of nearly pure *E2* multipolarity with $\delta \sim -3.0$ and would yield a much larger a_4 coefficient of $+0.30$. A rather weak ($\sim$1%) ground-state decay branch of 2277 keV was observed in the

TABLE II. Relative change of the ^{64}Ni and ^{66}Ni level population in reactions selected by using appropriate coincidence relationships described in the text. Column 1 in both halves of the table lists the energies of the main transitions deexciting the states for which the spin assignments are given in column 2. Note that the levels are ordered starting from the yrast sequence followed by nonyrast levels given in order of increasing excitation energy. The $I^{\gamma}_{Q}/I^{\gamma}_{\mathrm{TOT}}$ values represent ratios of peak areas observed in spectra selected for ^{64}Ni or ^{66}Ni nuclei produced in quasielastic reactions (Q) and in spectra representing a nonselective integral (TOT) population of these nuclei. The double-coincidence gates placed on the ^{238}U and ^{236}U ground-state band γ rays selected the ^{64}Ni or ^{66}Ni transitions populated in quasielastic reactions (Q), respectively, and the twofold coincidence spectra with single 1346- or 1425-keV $2^+ \rightarrow 0^+$ transition gates were used to determine the respective integral population (TOT) in ^{64}Ni and ^{66}Ni. The $I^{\gamma}{}_{\mathrm{CaU}}/I^{\gamma}{}_{\mathrm{NiU}}$ ratios listed in column 4 of both panels were calculated using peak areas in nonselective (TOT) spectra obtained with respective single gates on the $2^+ \rightarrow 0^+$ transitions measured for the ^{48}Ca + ^{238}U and ^{64}Ni + ^{238}U reactions (see text). These ratios have been normalized to the population ratios measured for the respective 4^+ yrast states, which were defined as unity. The values of these ratios observed for the yrast sequences illustrate most clearly the change in population mechanism by selected reactions. Conclusions drawn from the observed ratios are discussed in the text.

^{64}Ni				^{66}Ni			
E_γ (keV)	$I_i{}^{\pi}$	$I_Q{}^{\gamma}/I_{\mathrm{TOT}}{}^{\gamma}$	$I^{\gamma}{}_{\mathrm{CaU}}/I^{\gamma}{}_{\mathrm{NiU}}$	E_γ (keV)	$I_i{}^{\pi}$	$I_Q{}^{\gamma}/I_{\mathrm{TOT}}{}^{\gamma}$	$I^{\gamma}{}_{\mathrm{CaU}}/I^{\gamma}{}_{\mathrm{NiU}}$
1264.3	4^+	1.00*	1.00*	1760.2	4^+	1.00*	1.00*
1239.0	5^-	0.27(1)	1.86(6)	355.8	5^-	0.84(5)	1.08(2)
323.4	6^-	0.27(2)	1.85(5)	490.2	7^-	0.66(6)	1.30(3)
359.4	7^-		2.86(10)	1085.7	8^+	0.27(6)	1.30(6)
1280.0	8^+	<0.10	3.15(36)	1404.8	10^+	<0.08	1.95(21)
930.8	2^+	1.31(3)	0.32(6)	1245.5	0^+	3.40(30)	0.19(17)
1521.5	0^+	2.32(13)	<0.30	1545.9	3^+	1.80(40)	0.73(23)
1626.4	(2^+)	1.30(30)	<0.30	1803.5	2^+	2.5(17)	<0.15
1637.0	(3^+)	0.90(10)	1.54(67)	1945.7	3^-	2.30(30)	0.57(7)
1680.1	0^+	2.38(19)	<0.3	2188.8	4^+	0.60(20)	1.34(11)
1819.9	4^+	0.69(7)	1.15(24)	2261.7	3^-	1.60(70)	1.50(70)
2049.9	4^+	0.79(8)	0.93(22)	2367.5	4^+	0.60(30)	1.07(15)
2213.7	3^-	0.91(9)	1.20(31)				

coincidence with lines feeding the 2^+_2 level as well as with the ^{238}U transitions. The low intensity of this *E2* branch to the ground state indicates a $B(E2)$ reduced transition probability smaller by a factor 5×10^3 than the corresponding $B(E2)$ value for the *E2* component of the 931-keV transition. Also, the 2972-keV level, populated with much smaller intensity than the 2^+_2 state, could be tentatively assigned as the 2^+_3 level, based on the three observed, nearly equal intensity, decay branches to both lower-lying 2^+ levels and the ground state. In the off-beam coincidence data, the population of this state was observed from ^{64}Co β decay and, moreover, the in-beam population ratios for the 1626-keV transition in Table II are very similar to those observed for the 931-keV line.

Two levels, with 2867- and 3026-keV excitation energies, were also found to be directly populated in ^{64}Co β decay. Both of these could be unambiguously assigned spin-parity 0^+, herewith confirming earlier tentative assignments [24]. Transitions of 1521 and 1680 keV, respectively, depopulate these states exclusively to the 2^+_1 level and no feeding from any higher-lying state was detected. The ratios of Table II clearly establish these levels as very low-spin, nonyrast states populated almost solely in quasielastic reactions. Most importantly, the angular-correlation results (see the example in Fig. 5) are fully consistent with the proposed $0^+ \rightarrow 2^+ \rightarrow 0^+$ sequences as they exhibit the characteristic large a_4 coefficient.

A 4^+ spin-parity was firmly assigned to the 3166- and 3396-keV levels as the present angular-correlation results are consistent with the previous unique 4^+ assignment reported for the former [19] while the coefficients listed for both the depopulating (2050- and 786-keV) and feeding (453-keV) transitions of the latter remove any earlier ambiguity. A weak transition of 230 keV connecting both 4^+ states could be observed and the respective population ratios of Table II are also consistent with the 4^+ assignment, taking into account a significant feeding from higher-spin states.

The spin-parity assignment to the previously unobserved level at 2983 keV is somewhat more complex. The angular-correlation coefficients for the 1637- and 707-keV depopulating transitions are rather inconclusive, but would be consistent with a hypothetical 4^+ assignment. At the same time, the population of such a low-lying 4^+_2 state would be expected to be stronger than the measured intensity. Also, the absence of an energy-favored feeding transition from the well-established 5^- level, which decays to the three other 4^+ levels, leads one to conclude that a 3^+ assignment is more likely. Strong support for such an assignment was provided by inspection of thermal neutron capture ^{63}Ni(n,γ) data [29]: A 1637-keV transition was observed in these (n,γ) data, but not placed in the level scheme. Although the more intense 707-keV $(3^+) \rightarrow 2^+$ line could not be detected due to spectral difficulties (contaminants), the quality of the data allows one to conclude that the 2983-keV ^{64}Ni level was populated in this (n,γ) measurement. Moreover, as expected for such a 3^+ assignment, the population of this level apparently proceeds via other states, because no primary transition feeding it from an initial 1^- state was observed. Such a primary decay feeding is observed for all the 0^+ and 2^+ states discussed above and for higher-lying states populated in the 1^+, ^{64}Co β decay,

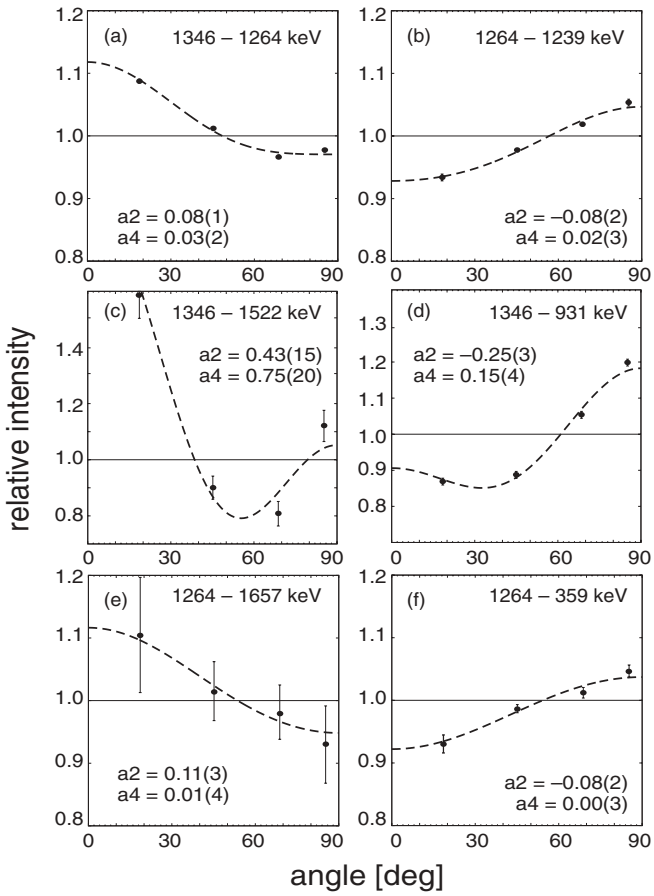

FIG. 5. Samples of γ-γ angular-correlation results obtained for ^{64}Ni in the present study. The energies of the analyzed transition pairs and the fitting results are indicated in each panel. A complete list of numerical results is provided in Table I.

as will be discussed in a forthcoming publication [27] and as was also observed in the present off-beam coincidence data. On the other hand, none of the ^{64}Ni 4^+ states could be detected in the (n,γ) data [29], reemphasizing the 3^+ tentative spin-parity assignment to the 2983-keV level. The same neutron capture data [29] established a fairly sizeable population for the 3463-keV state in the primary decay from a 1^- initial level. This level was very weakly populated in the present experiment, but clearly detected through the presence of the 1186-keV γ ray feeding the 2277-keV state, as seen in the coincidence spectrum of Fig. 3(d). Much higher population of this state in the thermal neutron capture reaction established a ~5-times-weaker 2117-keV transition to the 2^+_1 state, whereas the transition to the ground state was not observed. It should also be noted that no population of this level was observed in the 1^+, ^{64}Co β decay study [27]. Consideration of all these observations favors a 2^- spin-parity assignment to the 3463-keV level, but taking into account that the 2^- state is expected to be located at much higher energy (see Sec. IV), other possibilities cannot be strictly excluded and the $I^\pi = (2^\pm,3^-)$ tentative assignment is proposed.

The present results confirm the unique $I^\pi = 3^-$ assignment to the 3560-keV level which decays by two *E1* γ branches with very similar $B(E1)$ reduced transition probabilities to the two lowest 2^+ states. The $I^\pi = 4^-$ assignment to the 3749-keV level is based on angular-correlation results, which establish the respective $\Delta I = 1$ and $\Delta I = 0$ dipole character of the two strongest depopulating transitions of 189 and 583 keV. The assigned parity is strongly favored by the observed cascade of the 359-, 323-, 100-, and 189-keV *M1* transitions connecting negative-parity states in a $7^- \to 6^- \to 5^- \to 4^- \to 3^-$ decay sequence. All the other competing decay branches from these levels are consistent with strongly retarded *E1* transitions, showing fairly (within a factor of ~20) comparable $B(E1)$ reduced transition rates. Furthermore, a preference for *M1* decays between these negative-parity states is emphasized by a remarkable absence of competing *E2* branches. In fact, only in the case of the 3849-keV 5^- level, where the decay proceeds through a particularly low-energy 100-keV *M1* branch and three *E1* transitions, a very weak $5^- \to 3^-$ *E2* transition of 289 keV could be detected as well. To conclude on this issue, the strongly preferred *M1* character for the 100-keV line feeding from the 5^- state and of the 189-keV depopulating transition toward the 3^- level establish the 4^- spin-parity assignment to the 3749-keV level. In agreement with this assignment, three competing *E1* decay branches to lower-lying 4^+ and 3^+ states are observed while, at the same time, an energy-favored transition to the 2^+_1 state, which would be expected in the event of a positive parity assignment, remained unobserved with an intensity limit of 0.2 in the units of Table I.

New levels located at 4418 and 4477 keV were tentatively assigned as $3^\pm$, 4^+, and 6^+ states on the basis of their observed decays through a single transition and their population intensity which is consistent with weak feeding of such high-lying, nonyrast states.

B. ^{66}Ni

The present analysis has significantly expanded the ^{66}Ni level scheme established earlier [19] and provided firm spin-parity assignments for most of the observed states. In ^{238}U + ^{64}Ni collisions, ^{66}Ni is produced in $2n$ transfer and includes quasielastic processes as well as deep-inelastic reactions with subsequent neutron evaporation or fission of the targetlike fragments. Coincidence spectra displayed in Fig. 6 present a general view of transitions populated in ^{66}Ni while emphasizing features characteristic of both types of reactions in a way similar to that introduced above for ^{64}Ni. The upper spectrum [Fig. 6(a)] illustrates the yrast population and was obtained with double-coincidence gates placed on all combinations of the six strongest transitions observed in the yrast decay sequence. The ^{66}Ni transitions are marked by energies and cross-coincidence γ rays associated with the ^{236,235,234}U reaction partners are indicated by the symbols found in Fig. 6. Whereas these cross-coincidence transitions are clearly visible, one may conclude from their relatively low intensity that the bulk of the ^{66}Ni yrast population arises from processes involving fission of heavy fragments. The coincidence spectrum of Fig. 6(b) was obtained with double gates set on the 1425-keV, $2^+ \to 0^+$ transition together with the most intense lines in the ^{236}U ground-state band. Just as in the case of ^{64}Ni, the predominant nonyrast population selected

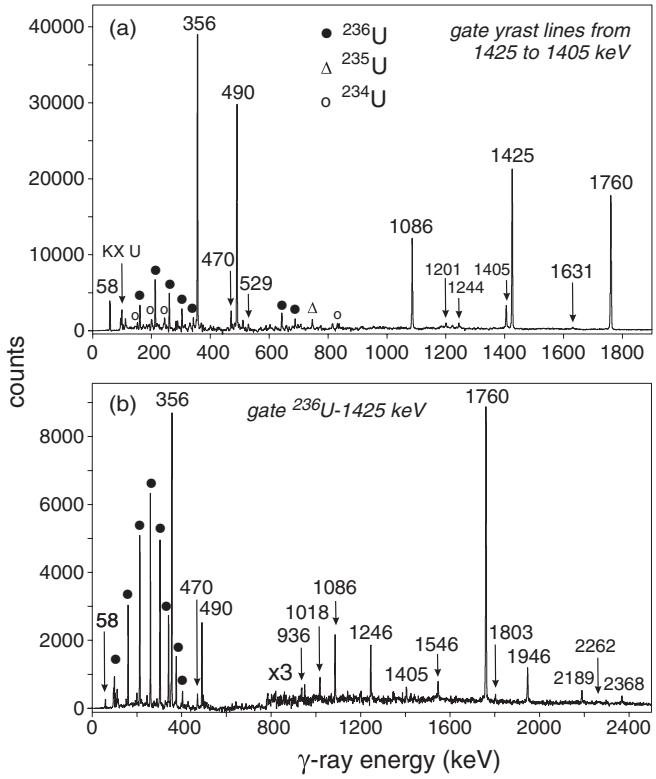

FIG. 6. Coincidence spectra obtained with double gates enhancing the observation of yrast (a) and nonyrast (b) states populated in ^{66}Ni. Spectrum (a) was obtained with double gates set on all pair combinations of the 1425-, 1760-, 356-, 490-, 1086-, and 1405-keV transitions from the ^{66}Ni yrast sequence. Spectrum (b) is the sum of coincidence spectra with gates placed on the 1425-keV, $2_1^+ \rightarrow 0^+$ γ ray together with the ^{236}U ground-state band transitions. ^{66}Ni transitions are indicated by their energies and lines from ^{236}U, ^{235}U, and ^{234}U reaction partners are marked by solid circles, open triangles, and open circles, respectively.

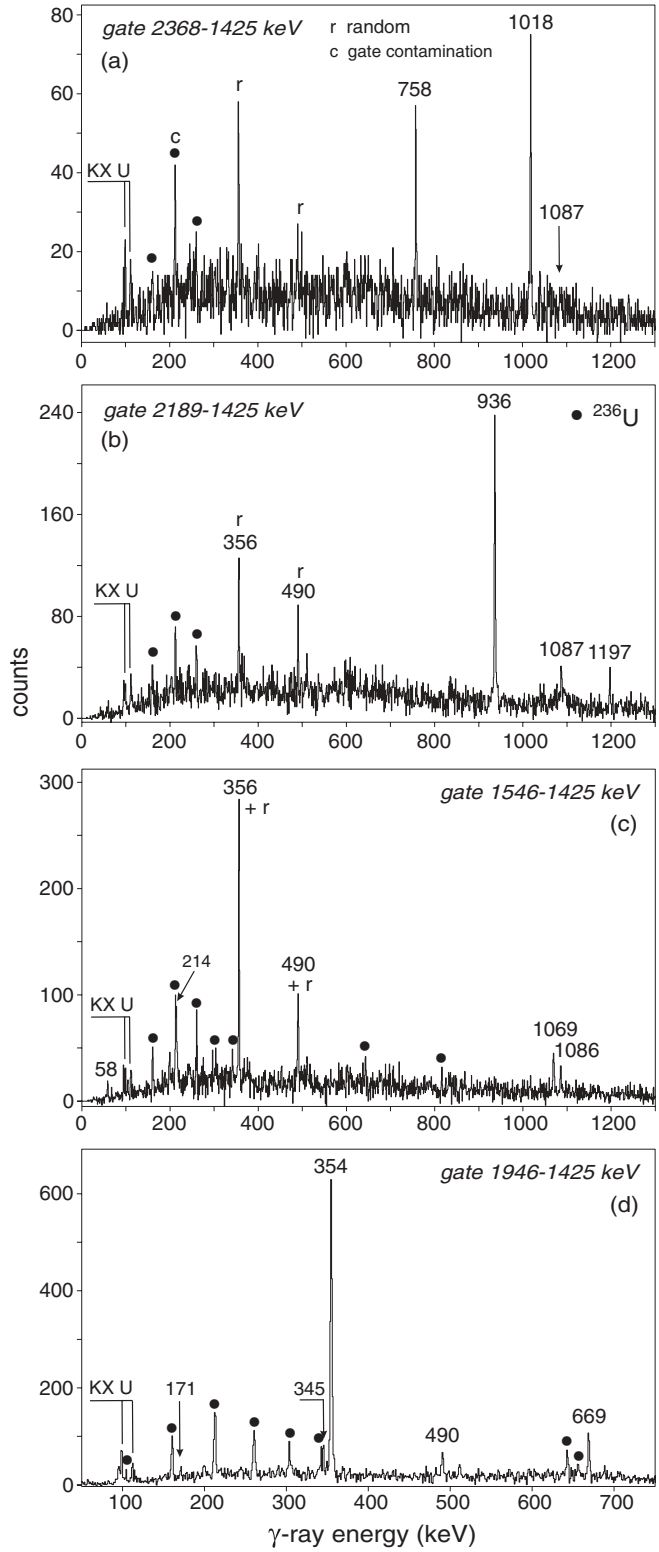

FIG. 7. Selected examples of coincidence spectra illustrating the population of nonyrast ^{66}Ni levels from higher-lying states. The energies of the gating pairs of transitions are indicated in each panel. Solid circles mark ^{236}U lines, random coincidences and gate contamination lines are marked with the letters r and c, respectively.

by this condition was instrumental in identifying levels in ^{66}Ni parallel to the main yrast sequence. These levels are represented by the high-energy γ rays marked in Fig. 6(b). Sample coincidence spectra displayed in Fig. 7 document some features used in the development of the nonyrast part of the level scheme.

Important observations changed the location of the 4.3-ns isomeric state in the ^{66}Ni level scheme from that proposed previously [19]: This is illustrated in Fig. 8. A dedicated sort of the data was undertaken to obtain PDD and DDD coincidence cubes with a rather narrow (8–45 ns) time window defining the delayed range. Despite the short half life of the isomer, a clear separation between transitions located above and below the isomer was achieved. The upper spectrum [Fig. 8(a)] displays prompt γ rays (from the PDD cube) preceding in time the 356-, 1425-, and 1760-keV delayed transitions selected by the three combinations of double gates indicated in the figure. In contrast, the lower spectrum [Fig. 8(b)] produced from the DDD cube under the same conditions confirms that the three gating lines involved represent the main decay path of the isomer. The noteworthy separation achieved between prompt and delayed transitions shows, perhaps surprisingly, that the low-energy 58-keV line is located above the isomer. It had

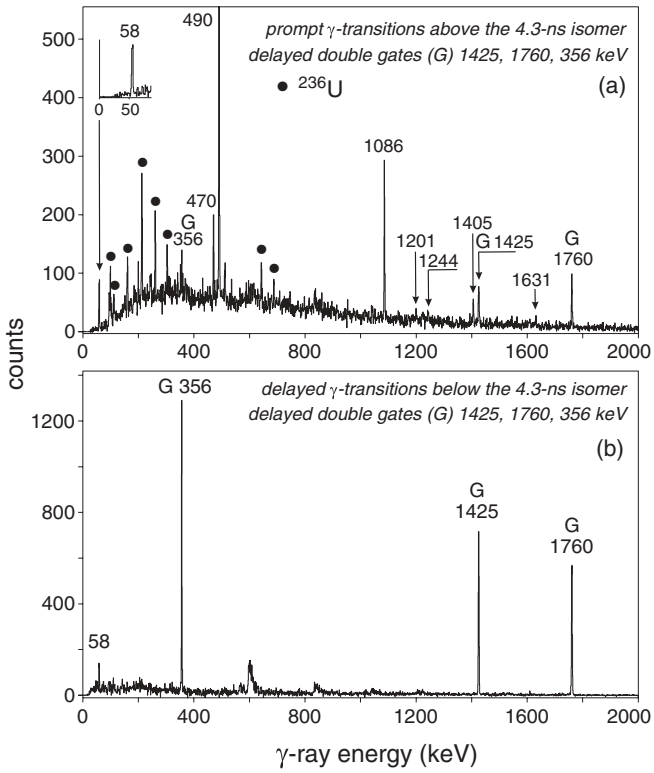

FIG. 8. Coincidence spectra documenting the location of the 4.3-ns isomer in ^{66}Ni. As discussed in the text, an 8- to 45-ns delayed time range was selected. Spectrum (b) was obtained by requiring three delayed γ rays and double gates set on combinations of the 1425-, 1760-, and 356-keV transitions. Spectrum (a) uses the same delayed double gates to enhance prompt γ lines preceding the isomer in time. The insert shows the crucial 58-keV transition and proves its location above the isomer (see text for details). The energies of ^{66}Ni transitions are indicated and the solid circles in (a) mark ^{236}U cross-coincidence γ rays.

previously been suggested that this transition was associated with the isomer decay [19], but its presence in Fig. 8(a) with a clearly enhanced intensity places it above the 4.3-ns isomeric state, and, in turn, defines the 356-keV transition as the main isomeric decay branch. It should be noted that the 58-keV transition would not be seen at all in the spectrum of Fig. 8(a) if it was placed below the isomer, because even for higher-energy γ rays the leakage of prompt coincidences is substantially reduced (see intensities of the 356-, 1425-, and 1760-keV lines in the same spectrum). However, the presence of a weak 58-keV line in Fig. 8(b) is attributed to the poor timing properties of large-volume HPGe detectors at low energy, which shift some of this line's intensity to the delayed time range. In the search for the 529-keV transition, which should also precede in time the isomeric decay, only traces of such a line were found in the spectrum of Fig. 8(a), but with a number of counts compatible with the expected intensity.

The ^{66}Ni level scheme established in the present work is displayed in Fig. 9 and Table III provides information on transition energies and intensities as well as on angular correlations. Quantitative results showing the relative change in the ^{66}Ni nonyrast and yrast state population by the various reaction mechanisms are found in Table II, which was introduced and discussed in Sec. III A above (see the table caption for further details). They provided additional information in support of the spin-parity assignments based mainly on the angular-correlation coefficients listed in Table III. Representative examples of angular-correlation results for ^{66}Ni transitions are presented in Fig. 10.

The present analysis of the γ-coincidence data confirmed the previously proposed level scheme [19] for the main yrast sequence and extended it by a single transition (1631 keV) which establishes the highest-energy level observed in the present work at 8211 keV. In the upper part of the scheme, two other weak transitions of 1244 and 1201 keV could be observed and assigned as single transitions depopulating new states at 5334 and 6376 keV, respectively. No spin and parity quantum numbers are proposed for these two levels as the small intensity did not provide the opportunity to derive angular-correlation information from the data. The 4069-keV level, which was established earlier [19] by a single 470-keV depopulating transition, was confirmed here through the observation of four additional, less intense decay branches (Fig. 9). Also, in the present data, no population of this 4069-keV state from higher-lying, discrete states could be detected.

The angular-correlation coefficients determined for the main yrast transitions (Table III) provide firm spin-parity assignments of 4^+, 5^-, 6^-, 7^-, 8^+, and 10^+ to the 3185-, 3541-, 3599-, 4089-, 5175-, and 6580-keV levels, respectively. In this instance, some parity assignments were also guided by straightforward shell-model expectations making it possible to attribute a most likely parity in various spin and excitation-energy regions of the yrast sequence. Somewhat surprising is the nearly isotropic correlation observed for the 490-keV, $7^- \rightarrow 6^-$ transition as measured in coincidence with the 1425- and 1760-keV $E2$ transitions. Consideration of any other assignment than 7^- to the 4089-keV level would pose difficulties in the interpretation of these results and, therefore, it was concluded that the 490-keV transition is of mixed $M1/E2$ character with a value $\delta = -0.1$, yielding angular correlation coefficients consistent with the experimental values.

Compared to previous results [19,25], the nonyrast part of the ^{66}Ni level scheme was significantly expanded and several spin-parity assignments were changed. The 4069-keV level is assigned as a 5^- state on the basis of the dipole character inferred for the 470-keV line from angular-correlation results. A 7^- assignment is excluded based on the clear nonyrast population of the state and on the observed decay branches to other lower-lying states, specifically to $I = 4$ levels. The most dramatic change in assignment concerns the third excited state at 2671 keV, which was suggested earlier to be a 3^+ level and is unambiguously assigned here as the $I^\pi = 0_3^+$ state. The angular-correlation results listed in Table III and displayed in Fig. 10 for the 1246-keV depopulating transition are strongly supportive of this 0^+ assignment. Consequently, the observed population of this state in β decay leads one to question the tentative 3^+ assignment proposed for the ground state of the ^{66}Co mother nucleus [25]. The 2664(10)-keV 0^+ state populated strongly in the (t,p) reaction [30] is apparently identical to the 2671-keV level assigned in the present work.

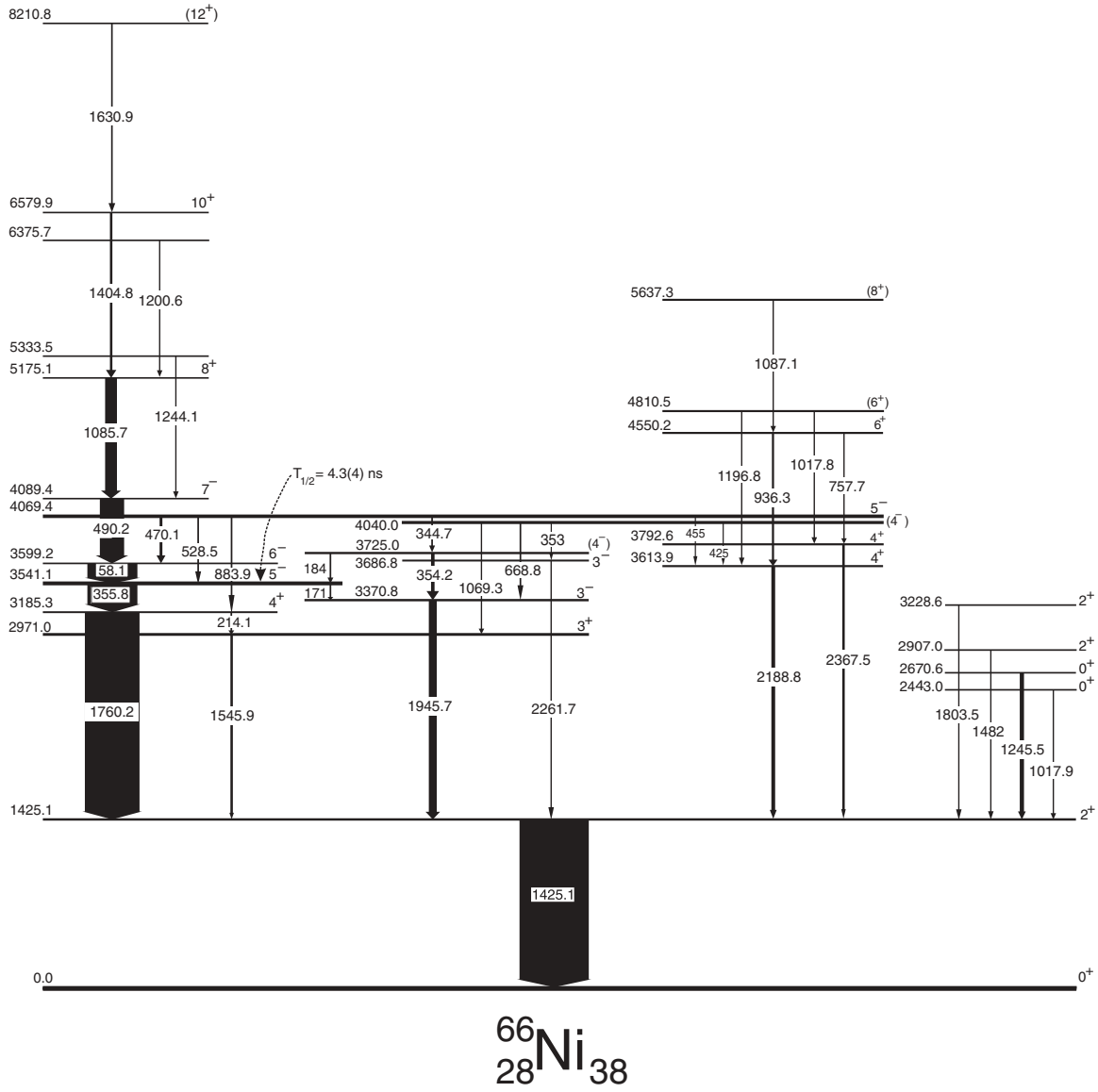

FIG. 9. ^{66}Ni level scheme established in the present study. The widths of the arrows reflect the observed transition intensities for the strongest transitions only. The spin-parity assignments are discussed in detail in the text.

Moreover, the population ratios for the 1246-keV transition in Table II indicate firmly the enhanced population of this 0_3^+ state by $2n$ transfer in quasielastic reactions and the lack of feeding by deep-inelastic reactions in the $^{48}\mathrm{Ca} + ^{238}\mathrm{U}$ experiment.

An $I^\pi = 3^+$ spin-parity is now assigned to a state located at 2971 keV (Fig. 9). Although angular-correlation results are inconclusive for the 1546-keV γ ray, the population ratios observed for this transition (Table II) are consistent with the proposed 3^+ assignment. Important additional support is provided by the observation of a weak 214-keV transition from the 3185-keV, 4^+ state representing a low-energy *M1* deexcitation able to compete with the high-energy 1760-keV *E2* decay. Note that a 2965(10)-keV level was weakly populated in the (t,p) reaction of Ref. [30], where it was assigned as a 0^+ state. However, taking into account a systematic energy shift of -6 keV that seems to affect these (t,p) data, this level can likely be associated with the 2971-keV, 3^+ level under discussion here and the reported small (t,p) cross section as well as the presently observed weak population would then be consistent with such an assignment.

The $I^\pi = 3^-$ assignment proposed for the 3371-keV level on the basis of the (t,p) data [30] is confirmed here by the angular-correlation results extracted for the 1946-keV depopulating transition as well as by the corresponding population ratios of Table II, which confirm a low spin value. A weak 171-keV transition linking this level with the 3541-keV, 4.3-ns, 5^- isomer is understood as an *E2* transition [$B(E\ [2]) = 2(1)$ W.u.] competing with a retarded 356-keV *E1* decay [$B(E1) = 2 \times 10^{-6}$ W.u.]. The two higher-lying states at 3725 and 4040 keV feed predominantly the 3371-keV, 3^- level and are tentatively assigned $I^\pi = 4^-$.

TABLE III. Same as Table I, but for ^{66}Ni. Transition intensities have been normalized to the population of the 1425.1-keV, 2_1^+ state. Angular-correlation coefficients with the relevant gating transitions are given in the last three columns. Gating transitions with multipolarities other than *E2* are marked with a * sign.

E_{level} (keV)	I^π	E_γ (keV)	I_γ (rel.)	a_2	a_4	Gate
1425.1	2^+	1425.1(1)	100			
2443.0	0^+	1017.9(3)	0.9(3)			
2670.6	0^+	1245.5(2)	4.5(6)	0.29(6)	0.83(10)	1425
2907.0	2^+	1482.0(15)	0.2(2)			
2971.0	3^+	1545.9(2)	2.7(5)	−0.04(5)	–	1425
3185.3	4^+	214.1(4)	1.1(5)			
		1760.2(1)	76.2(3)	0.09(1)	0.03(2)	1425
3228.6	2^+	1803.5(3)	0.9(4)			
3370.8	3^-	1945.7(1)	6.9(2)	−0.07(3)	0.02(4)	1425
3541.1	5^-	171.1(5)	0.2(1)			
		355.8(1)	72.7(4)	−0.08(1)	0.02(1)	1425
				−0.09(1)	0.02(1)	1760
3599.2	6^-	58.1(2)	36.2(3)	−0.07(3)	0.07(5)	1760
3613.9	4^+	2188.8(3)	5.5(5)	0.10(4)	0.05(6)	1425
3686.8	3^-	2261.7(4)	0.5(3)			
3725.0	(4^-)	184.1(2)	0.7(1)			
		354.2(2)	3.4(5)	0.02(6)	0.06(8)	1946*
3792.6	4^+	2367.5(3)	2.9(4)	0.04(10)	–	1425
4040.0	(4^-)	353	0.2(2)			
		425.4(6)	0.2(1)			
		668.8(3)	0.9(3)			
		1069.3(4)	1.3(3)			
4069.4	5^-	344.7(4)	0.3(2)			
		455.2(3)	0.2(1)			
		470.1(2)	3.8(5)	−0.11(5)	–	1425
				−0.05(3)	–	1760
		528.5(4)	1.1(5)			
		883.9(4)	1.0(3)			
4089.4	7^-	490.2(1)	32.3(3)	0.05(1)	0.02(1)	1086*
				0.02(1)	0.02(1)	1760
				0.00(1)	0.01(1)	1425
4550.2	6^+	757.7(3)	0.8(3)			
		936.3(2)	3.2(2)	0.18(9)	–	1425
				0.07(9)	–	2189
4810.5	(6^+)	1017.8(3)	1.0(3)			
		1196.8(4)	0.4(1)			
5175.1	8^+	1085.7(1)	15.9(2)	−0.09(2)	0.02(2)	1425
				−0.11(4)	0.02(4)	1760
5333.5		1244.1(3)	1.0(3)			
5637.3	(8^+)	1087.1(4)	0.6(1)			
6375.7		1200.6(4)	0.6(2)			
6579.9	10^+	1404.8(3)	4.0(1)	−0.05(1)	0.02(1)	1086*
				0.15(7)	–	1425
8210.8	(12^+)	1630.9(4)	0.3(1)			

For the 354-keV line, the strongest transition depopulating the 3725-keV level, only the 1946-keV coincidence gate could be used for the angular-correlation analysis as an unwanted interference by a dominating, close-lying 356-keV γ ray needed to be avoided. The measured correlation coefficients (Table III) are consistent with the 354-1946-keV cascade being of dipole-dipole character, but are not conclusive in view of the associated uncertainties. Nevertheless, the observed 184-keV parallel decay branch to the 3541-keV, 5^- level as well as the weak population by a 345-keV line from the 4069-keV, 5_2^- state, which mirrors closely the dominance of *M1* transitions between negative-parity states in ^{64}Ni discussed above, also favor the proposed 4^- assignment for the 3725-keV level. The decay branches observed for the 4040-keV state and the absence of any discrete feeding from higher-lying states suggest a similar, but tentative, 4^- assignment.

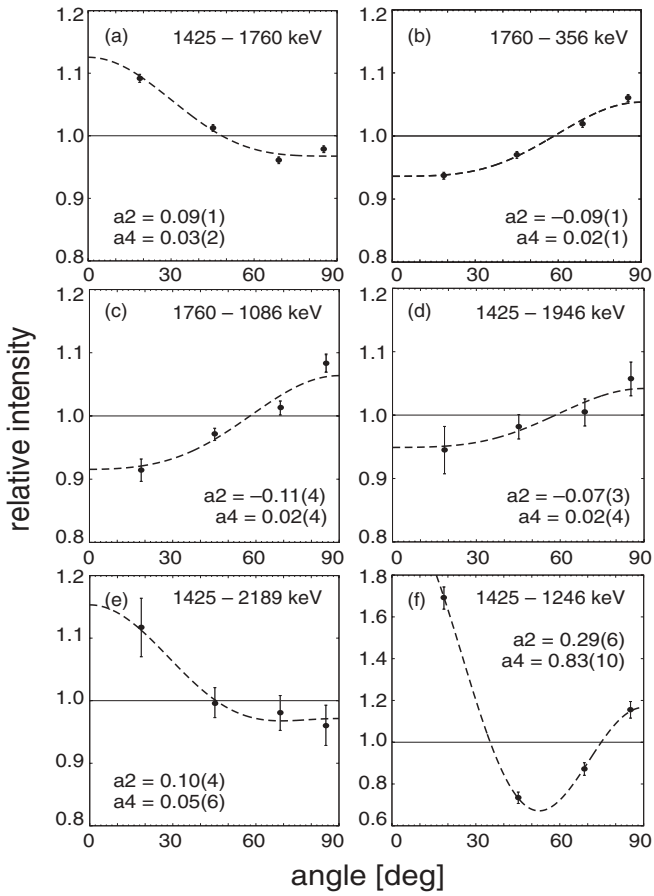

FIG. 10. Examples of γ-γ angular-correlation results obtained for ^{66}Ni in the present study. The energies of the analyzed pairs of transitions and the fitting results are indicated in each panel. A complete list of numerical results is given in Table III.

The nonyrast nature of the 3229- and 3687-keV levels is supported by the measured population ratios of Table II. Both states were also observed in the (t,p) reaction [30] and they are assigned here as 2^+_3 and 3^-_2 states, respectively. Moreover, the 3229-keV level is populated in ^{66}Co β decay and, accordingly, was observed in the present analysis of γ-γ off-beam events, herewith supporting the 2^+ assignment. In the case of the 3687-keV level, a weak transition of 353 keV feeding this level from the 4040-keV (4^-) state is also consistent with a 3^- assignment that is essentially based on the (t,p) data of Ref. [30].

A more extensive population of nonyrast states was observed above the two levels assigned as $I^\pi = 4^+$ located at 3614 and 3793 keV, respectively. Both states can possibly be correlated with the 3605(10)- and 3782(10)-keV levels reported in the (t,p) reaction, although no spin-parity assignment was proposed [30]. The angular-correlation coefficients extracted for the 2189-keV transition uniquely assign 4^+ quantum numbers to the 3614-keV level. A less conclusive angular-correlation result was obtained for the weaker 2368-keV line. However, the observed population from the 6^+_2 state, discussed below, supports the 4^+ assignment to the 3793-keV level.

The previously unobserved levels at 4550 and 4811 keV are assigned as $I^\pi = 6^+$. Each of these decays selectively to both nonyrast 4^+ states, whereas decay branches to the 3185-keV yrast 4^+ state could not be observed. The angular-correlation coefficients establish the stretched-$E2$ multipolarity of the 936-keV γ ray and result in a firm 6^+ assignment to the 4550-keV level. The observed 758-keV parallel decay branch then requires the 4^+ assignment to the 3793-keV level considered above. In the case of the 4811-keV state, a similar 6^+ assignment remains tentative as it is based mainly on the observed analogy with the lower 6^+ level, when considering the pattern exhibited by the γ decay and the population intensity for such nonyrast states. Within this group of states showing a clear structural relation through their observed γ-decay selectivity, yet another state could be located at 5637 keV. The observed population intensity and the 1087-keV decay transition to the lower-lying 6^+_1 state suggest an $I^\pi = 8^+$ most likely spin-parity assignment for this level.

A dedicated search was carried out to verify whether the 0^+ level at 2445 keV and the 2^+ state at 2916 keV, firmly established in the (t,p) reaction study [30,31], are populated in the present experiment as well. As the uncertainty of level energies in the (t,p) reaction study was estimated to be 10 keV, the quoted level energies are those adopted in the NDS compilation [25] on the basis of two γ transitions observed in the early study of ^{66}Co β decay [32]. However, a subsequent study of this radioactive decay did not detect such γ rays [33] and a more precise energy determination of both levels required in the present search was obtained in another way. Comparisons of level energies established in the (t,p) reaction [30] with the much more accurate ones obtained from the present study, indicated a systematic shift of $\Delta E = -6$ keV between the two measurements. Consequently, the expected level energies should be close to 2443 and 2906 keV for the 0^+_2 and 2^+_2 states located originally in the (t,p) reaction study at 2437(10) and 2900(10) keV, respectively. The expected γ transitions to the 1425-keV 2^+_1 level should then have corresponding energies of 1018 and 1481 keV, respectively. Indeed, in the crucial coincidence spectrum obtained with double gates placed on the 1425-keV γ ray and the ^{236}U transitions of Fig. 6(b), the 1018-keV line is clearly present with the precise peak position of 1017.9 keV. It is nearly 1 keV higher than the 1017.0-keV energy of the strong ^{65}Ni transition which could potentially contribute via random coincidences. However, it is completely unresolved from the 1017.8-keV transition located in the upper part (4810-keV level) of the ^{66}Ni level scheme. The latter contribution could be safely estimated by the intensities of the 758-, 936-, and 1197-keV transitions which are placed in the same region of the ^{66}Ni level scheme and are observed in the same spectrum. It was concluded that the bulk (2/3) of the 1017.9-keV line seen in Fig. 6(b) represents the $0^+_2 \rightarrow 2^+_1$ transition depopulating the first excited 0^+ state established in the (t,p) reaction [30,31]. Accordingly, the presently established 2443.0(3)-keV level energy and the 0.9(3) relative intensity of the 1017.9-keV depopulating transition are listed in Table III. Why this first excited 0^+ state is populated approximately 5 times less than the second excited 0^+ level at 2671 keV in quasi-elastic,

$2n$ transfer following ^{64}Ni + ^{238}U collisions remains an open question.

A trace of the 1482-keV line could also be seen in the spectrum of Fig. 6(b). However, it can hardly be considered as evidence for the population of the 2_2^+ state established in the (t,p) reaction [30,31] with the expected precise energy of 2907 keV. In Table III this level is also listed with an estimated upper intensity limit for the 1482-keV depopulating transition. It has to be noted that the possible short lifetime of this state may be responsible for this rather weak evidence.

Finally, whereas the most recent ^{66}Co β-decay study will provide a full account of the levels populated in ^{66}Ni [27], the inspection of the off-beam data from the present experiment, as well as from the earlier ^{48}Ca + ^{238}U measurement, revealed a sizeable population of the ^{66}Co isotope. Apart from the levels established previously in this decay [33], the analysis also indicated a weak, but consistent presence of the 1018- and 1482-keV lines in coincidence spectra obtained with the gate placed on the 1425-keV, ^{66}Ni transition when the trigger condition was relaxed to twofold coincidences. The population of these 0_2^+ and 2_2^+ levels under discussion here would be consistent with the 1^+ assignment to the ground state of the ^{66}Co mother nucleus. Furthermore, the small intensity of these decay branches probably carries significant information on the structure of the populated states.

C. ^{68}Ni

The production of the more neutron-rich ^{68}Ni isotope under the present experimental conditions results in a reaction yield much smaller than that observed for the lighter even-mass Ni isotopes and the population pattern also favors higher-spin states. Nevertheless, the high statistics accumulated in the present measurements stimulated efforts to search for additional information on this relatively well-known nucleus.

The earlier ^{68}Ni studies started with the observation of a 0^+ first-excited state [3] which was later followed by the identification of the high-energy 2_1^+ level and of the 0.86-ms, 5^- isomer [4]. These observations were all viewed as indications of an $N = 40$ subshell closure. Subsequent discovery of a 23-ns, 8^+ isomer with a fairly complex γ decay [6] and the β-decay study of two ^{68}Co isomers with 7^- and 3^+ suggested assignments [33] added to the information on ^{68}Ni levels available prior to the current study and compiled recently in Ref. [34]. However, it should be noted that the recent investigation of Ref. [35] proposes tentative $I^\pi = 1^+$ quantum numbers for the second isomer in ^{68}Co.

The analysis was initiated with a search for prompt γ transitions feeding the 2_1^+ state. The high-energy, 2033-keV gate selected from the double-coincidence data provided a clean spectrum showing mainly the 1115-, 851-, and 209-keV transitions established earlier. Their rapidly decreasing intensities confirmed their ordering in the level scheme. For the strongest transition at 1115 keV a meaningful angular-correlation result could be obtained and the $a_2 = 0.12(6)$ coefficient extracted for the 2033-1115-keV pair strengthened the earlier assignment as a $4^+ \rightarrow 2^+ \rightarrow 0^+$ sequence. Apart from these three yrast transitions in the 2033-keV gated coincidence spectrum, only a 709.8(3)-keV line could be

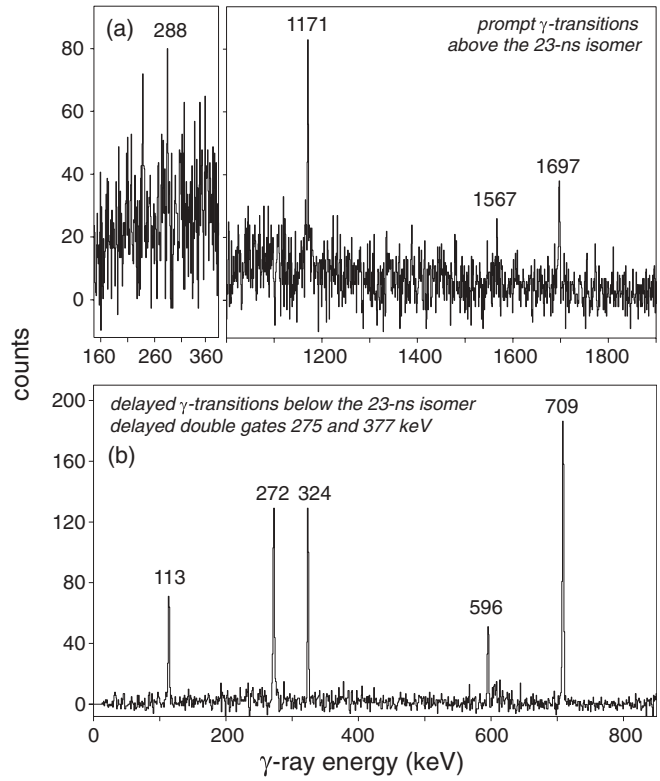

FIG. 11. Examples of coincidence spectra for ^{68}Ni transitions. Spectrum (b) was obtained by requiring three delayed γ rays with a double gate placed on the 275- and 377-keV transitions representing one branch of the 23-ns, 8^+ isomeric decay. Spectrum (a) displays prompt γ lines selected by setting delayed double gates on all coincident transition pairs below the 8^+ isomer. The ^{68}Ni transitions identified as preceding in time the 23-ns isomeric decay are indicated by their energies.

observed with an intensity lower by a factor of 4 compared to that of the 1115-keV γ ray. Apparently, this line represents a transition from the 2743-keV level observed in the ^{68}Co β decay of the low-spin (3^+) isomer which was tentatively assigned as the 2_2^+ state [33]. The competing ground-state decay from this level observed in Ref. [33] could not be seen in the present data. On the other hand, taking into account its reported intensity [33] leads one to conclude that this 2_2^+ level is populated nearly as strongly as the 3147-keV, 4^+ state. However, no evidence was found for the 478-keV transition from the 2511-keV level established earlier [33], where it was tentatively assigned as the 0_3^+ state. The population of such a state was estimated to be lower than 4% of the 3147-keV 4^+ state population.

The decay of the 23-ns, 8^+ isomer was analyzed with an optimized selection of the time range for delayed events. The quality of the data is demonstrated by the double-gated coincidence spectrum of Fig. 11(b). The present analysis fully confirmed the previously established decay scheme [6] and, moreover, verified its completeness, except for one additional crossover transition of 1086 keV connecting the 3933-keV level with the long-lived isomer at 2847 keV. In Table IV, the energies and intensities from the present work are listed for all transitions associated with this isomeric decay. These data are

TABLE IV. Energies and intensities of ^{68}Ni delayed transitions observed in the decay of the 23-ns, 8^+ isomer and of prompt γ rays located below and above this long-lived state. Intensities of delayed transitions were normalized to the total isomer decay defined as 100. For prompt transitions, 100 intensity units were arbitrarily assigned to the 1114.5-keV transition. In the delayed part, the negative result of a search for any other γ transition connecting the known states established an upper intensity limit of 0.4 units (see text).

E_γ (keV)	I_γ (Off-beam)	I_γ (In-beam)	$I^\pi{}_i$	E_{level}(keV)
113.1(1)	18.7 (16)		(6^-)	3555.8
209.3(1)	36.6 (24)	20.0 (15)	8^+	4207.9
257.9(3)		9.3 (21)	(4^+)	3405.4
271.6(2)	12.8 (15)		(4^-)	3118.9
274.7(1)	54.4 (30)		8^+	4207.9
287.5(5)		8 (2)[a]	(13^-)	7759.8
323.6(2)	10.8 (16)		(5^-)	3442.6
377.4(1)	39.9 (20)		7^-	3933.2
477.9(5)		<3	0^+	2510.8
595.5(2)	10.5 (16)		(5^-)	3442.6
652.2(2)	9.1 (15)		8^+	4207.9
663.2(3)		10.6 (18)	(4^+)	3405.4
708.6(1)	33.0 (20)		(6^-)	3555.8
709.8(3)		25.9 (25)	2^+	2742.7
814.4(1)	240 (30)		5^-	2847.3
851.2(1)	13.3 (15)	46.7 (35)	6^+	3998.6
1085.8(2)	13.7 (22)		7^-	3933.2
1114.5(1)	16.0 (16)	100.0*	4^+	3147.4
1151.3(1)	21.9 (20)		6^+	3998.6
1170.6(5)		20 (4)[a]	(9^-)	5378.5
1268.6(4)		7.6 (7)	(3^-)	3301.5
1445.0(9)		16 (4)[a]	(9^-)	5378.5
1567.0(9)		8 (2)[a]	(12^+)	7472.2
1697.3(5)		22 (4)[a]	(10^+)	5905.2
2032.9(2)	14.7 (14)	>140*	2^+	2032.9

[a]Prompt intensities of transitions above the isomer which were determined from selected double prompt gates and renormalized accounting for all isomer decay branches. For transitions located between the $8+$ and $5-1$ isomers, data were too complex to extract prompt intensities.

in many instances more precise than those reported earlier [6], but there is good overall agreement. It has to be noted that, apart from the above-mentioned 1086-keV γ ray, a search for any other new, weak transition connecting established levels, and possibly changing or clarifying the level ordering, was negative and resulted in a general estimate of an upper intensity limit for any unseen γ ray of 0.4 in the units of Table IV.

The ^{68}Ni level scheme is presented in Fig. 12. The level ordering below the 23-ns isomer is determined well, confirmed also by the β-decay results [33] so that the only possible remaining issue concerns the ordering of the 272- and 324-keV pair of transitions for which the presently adopted sequence is based solely on the intensities measured in β decay. The spin-parity quantum numbers in the level scheme (Fig. 12) essentially adopt the assignments of Ishii *et al.* [6], with the negative-parity states being assigned based mostly on the analogy with features of the γ decay observed for similar states in ^{64}Ni and ^{66}Ni.

The new result obtained in the present study concerns states located above the 8^+ isomer. The coincidence spectrum from the PDD cube, displayed in Fig. 11(a), presents prompt γ rays preceding in time delayed double-gated pairs of all transitions below the isomer. Four lines, indicated by their energies in Fig. 11(a), have been identified as ^{68}Ni transitions feeding this long-lived state; the relevant information on these transitions is also listed in Table IV. The analysis of double-prompt coincidence events (PPD) selected with single delayed gates placed on all transitions below the isomer established the mutual coincidence of the 1697-, 1567-, and 288-keV lines. In the yrast sequence of the level scheme (Fig. 12), the placement of the 1697-keV transition reflects its larger intensity, while the ordering of the equal-intensity 1567- and 288-keV lines is less certain, but is proposed under the assumption that the (much) lower-energy 288-keV transition is more likely to involve decay from a state with a lifetime >1 ps that enables the observation of narrow γ lines, free of Doppler broadening for the cascade. No other transition was found in prompt coincidence with the 1171-keV γ ray. As a result, the latter was placed just above the isomer establishing the 5378-keV level. A careful inspection of the PPP cube, with all double gates set on transitions below the 7^- level at 3933 keV, revealed the presence of the 1445-keV line with an intensity similar to that of the 1171-keV γ ray. Because no trace of such a line could be found in any similar double-gated coincidence spectra involving the 275-keV, $8^+ \rightarrow 7^-$ transition and because the energy matched well the 3933–5378 level spacing, the 1445-keV γ ray was placed as a parallel branch in the decay from the 5378-keV state. The suggested spin-parity assignments, indicated in Fig. 12, are tentative and based solely on the observed deexcitation pattern and on yrast-feeding considerations. For example, based on simple shell-model expectations, the highest-spin state in this energy range can arise from the maximal spin coupling of three $g_{9/2}$ neutrons and an $f_{5/2}$ neutron hole, a consideration leading to the $I^\pi = 13^-$ tentative assignment for the 7760-keV level.

In a recent publication, Dijon *et al.* [36] reported the discovery of a new isomeric state in ^{68}Ni with a 216(66)-ns half-life and a 168-keV decay γ ray to the 2033-keV 2_1^+ level. The authors assigned this isomer as the second excited 0^+ state and, because of its location just above the 2_1^+ level, proposed that it corresponds to a highly deformed proton intruder state. The evidence was based on the *A*/*Z* identification of ^{68}Ni products following a ^{238}U + ^{70}Zn reaction carried out in inverse kinematics. However, due to the low detector efficiency, the placement of the 168-keV γ ray and its assignment to ^{68}Ni could not be supported by the coincident detection of the 2033-keV, $2_1^+ \rightarrow 0^+$ line. A search for this isomer was undertaken using data from experiments performed with ^{48}Ca, ^{64}Ni, and ^{76}Ge beams on thick ^{238}U targets at energies ∼25% above the Coulomb barrier. Although the population of excited 0^+ states in ^{68}Ni is expected to be low in reactions with the beams listed above, a high detection sensitivity which exploits the selectivity of the 2033-keV gate in the delayed coincidence events (DD matrices) resulted in a reasonable probability for a successful search. In all γ-γ coincidence spectra with both the 2033-keV gate and the appropriately selected delayed time range, no evidence

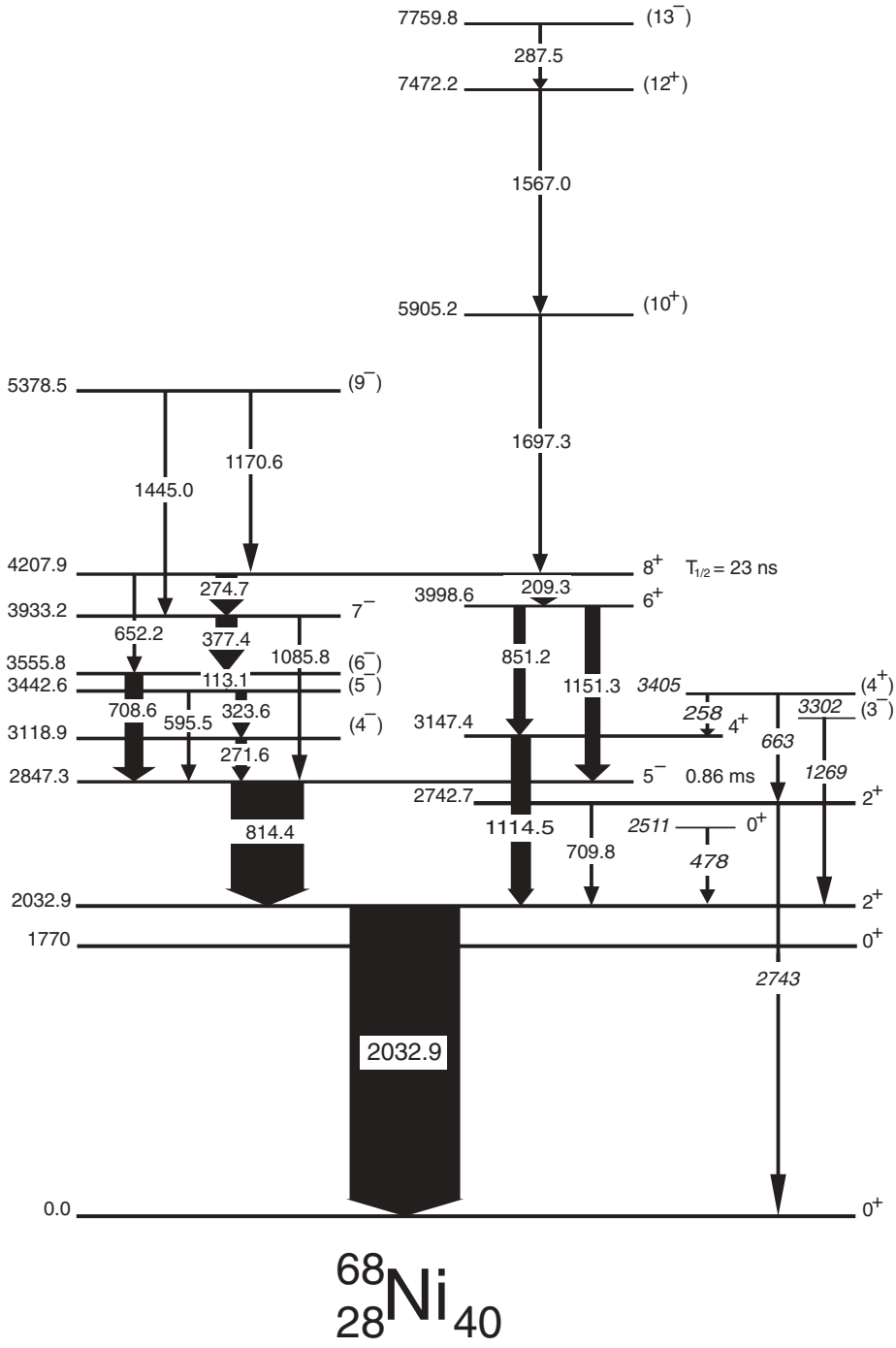

FIG. 12. The ^{68}Ni level scheme established in the present study. The spin-parity assignments are discussed in the text. Level and transition energies marked with italics were identified in Ref. [37] and confirmed in the present data, except for the weak 2743- and 478-keV transitions which could not be observed here.

was found for a 168-keV γ ray. With the intensity of the strong 814-keV transition from the long-lived 5^- isomer as a reference, the apparent absence of the 168-keV line could be quantified as a 0.4% upper limit of the 5^- state population observed within the delayed time window. The same lower limit for this 168-keV transition intensity was established recently in a similar analysis [37], but for the ^{70}Zn + ^{238}U reaction, that is, for the reaction used by the GANIL group [36].

The study of Ref. [37] quoted above used ^{197}Au and ^{208}Pb as well as ^{238}U targets with ^{70}Zn projectiles and established new, low-spin states at 3302 and 3405 keV in ^{68}Ni. It was thus interesting to verify whether these levels are also populated in the present ^{64}Ni + ^{238}U reaction. Starting from the identification in Ref. [37], the population of the 3405-keV level could be confirmed in the present work by observing two transitions at 663 and 258 keV, decaying to the 2743- and 3147-keV levels, respectively. Also, the presence of the 1269-keV line in the coincidence spectrum with the 2033-keV gate confirmed the population of the 3302-keV level. Both states are included in the level scheme of Fig. 12 and the corresponding transition energies together with the prompt intensities are listed in Table IV. The fact that these new levels are populated in a reaction favoring yrast states, excludes very low-spin values and supports the $I^\pi = 3^-$ and $I^\pi = 4^+$ tentative

assignments to the 3302- and 3405-keV levels, respectively. As expected for the 3^- assignment, the 3302-keV level decays by a single transition to the 2_1^+ state only, and is not populated in the β decays of neither the (3^+) or the (7^-) ^{68}Co isomers [33]. However, the 4^+ assignment for the 3405-keV level decaying to the 4_1^+ and 2_2^+ levels is consistent with the observation of a weak, though unplaced, 663-keV transition in the (3^+) ^{68}Co β-decay study [33]. For both states, no transition feeding from other known higher-lying states in ^{68}Ni could be detected.

IV. DISCUSSION: SHELL-MODEL CALCULATIONS AND INTERPRETATION OF ^{64}Ni, ^{66}Ni, AND ^{68}Ni LEVELS

The spectra of low-energy levels established in a series of odd-A Ni isotopes located between doubly magic ^{56}Ni and ^{68}Ni with its $N = 40$ subshell provide insight into structural changes taking place when successive neutrons fill the single-particle states available above the $N = 28$ closed shell. In ^{57}Ni, these neutron single-particle states are well separated with the ordering defined by the $p_{3/2}$ ground state followed by the $f_{5/2}$, $p_{1/2}$, and $g_{9/2}$ states with respective excitation energies of 768, 1113, and 4544 keV [38]. For heavier odd-A Ni isotopes, the corresponding shift of the Fermi level, combined with the presence of two-body interactions, results in a more complex situation where the negative-parity states are strongly mixed and more compressed in energy. In fact, the spectroscopic factors extracted from the available (d,p) data [39–42] indicate a large fragmentation of the single-particle amplitudes for the negative-parity states. The main feature that can be readily deduced from the data on these isotopes is the lowering in excitation energy of the $g_{9/2}$ state as the neutron number increases. This state stabilizes in excitation energy at around 1 MeV in ^{65}Ni and ^{67}Ni.

This apparent complexity of levels in odd-A Ni isotopes translates into difficulties using simple shell-model considerations to understand the observed level structure in even-Ni neighbors. It is clear that large-scale shell-model calculations are required to achieve a quantitative comparison with experimental levels. However, generally speaking, three groups of states should be expected in the level schemes. The first one regroups the lowest positive-parity states with spin values up to $I = 4$, which can be formed mainly by seniority-2 excitations involving the $p_{3/2}$, $f_{5/2,}$ and $p_{1/2}$ orbitals. The second group is that of negative-parity states ranging from $I = 2$ to $I = 7$ where one neutron is promoted to the $g_{9/2}$ orbital and couples with neutrons occupying the three lower, natural-parity states. Finally, all higher-spin states must arise from more complex excitations involving most often two or more $g_{9/2}$ neutrons.

In the earlier study of Ni isotopes in the $A = 64$–67 mass range [19], two different approaches were used to perform shell-model calculations in the full neutron (ν) $p_{3/2}$, $f_{5/2,}$ $p_{1/2}$ space with the occupation of the $g_{9/2}$ orbital limited to at most four neutrons. These two calculations used modified surface δ interactions and realistic sets of two-body matrix elements, respectively, with adjustments described in Ref. [19] and single-particle energies relative to the ^{56}Ni core adjusted to fit the Ni isotopes. Although, in Ref. [19], the experimental levels had no firm spin-parity assignments, the overall agreement between data and shell-model calculations up to an excitation energy of 6 MeV was judged to be satisfactory considering that the calculations (i) involved nuclei 8 to 11 neutrons removed from the ^{56}Ni core and (ii) neglected proton core excitations. However, it was pointed out specifically that the level order and the splitting of the two-particle $I^\pi = 5^-, 6^-, 7^-$ states with main configurations $\nu(g_{9/2}p_{1/2})$, $\nu(g_{9/2}p_{3/2})$, and $\nu(g_{9/2}f_{5/2})$ were poorly reproduced and that this observation was in marked contrast with the agreement achieved for the $\nu(g_{9/2})^2$, 8^+ state. This was attributed to the role of state mixing which affects relative positions and is an inherent consequence of the choice of residual interactions. As broadly discussed in Ref. [19], the issue of explaining the retarded $6^- \rightarrow 5^-$ $M1$ transition in ^{66}Ni was also raised as the latter was then suggested to be an isomeric decay in ^{66}Ni. As shown above in Sec. III B, this difficulty has now been resolved by strong experimental evidence assigning the isomeric 4.3-ns half-life to the 3541.1-keV, 5^- state.

Recently, large-scale shell-model calculations were carried out with the code ANTOINE [43,44] and were confronted with experimental levels in ^{67}Ni [18] and ^{65,67}Cu [23]. Assuming a ^{56}Ni core, the valence space was again restricted to the neutron $p_{3/2}$, $f_{5/2}$, $p_{1/2}$, and $g_{9/2}$ orbitals, but the required two-body interactions and single-particle energies were obtained from fits to two different sets of experimental data. The JUN45 effective interaction was obtained by Honma *et al.* [45] from fitting experimental energies of 69 nuclei near $Z = 28$ or $N = 50$ with masses $A = 63$ to 96. The Ni and Cu isotopes were excluded from the fit due to the expected softness of the ^{56}Ni core which might require the inclusion of the $f_{7/2}$ state in the valence space. The jj44b [46] interaction, however, incorporated experimental fit parameters from $^{57-78}$Ni and $N = 50$ isotones from Cu to Sn. Calculations with these two sets of interactions resulted in a satisfactory agreement between experiment and theory for ^{67}Ni [18] and ^{65,67}Cu [23]. These two sets of interactions were also used in the present work to compute the levels of ^{64,66,68}Ni. However, before discussing these results, it is worth pointing out some conclusions drawn for the ^{67}Ni nucleus in Ref. [18]; that is, for a case involving solely neutron excitations, which are also relevant for the understanding of the even Ni isotopes under consideration here. It was noted that with both interactions, particularly the JUN45 set, the energy of the $9/2^+$ state in ^{67}Ni was predicted to lie significantly lower than the experimental value, possibly indicating that the adopted $\nu g_{9/2}$ single-particle energy in the two Hamiltonians was too small. Consequently, the calculated higher-lying levels in ^{67}Ni were found to reproduce the experimental ones satisfactorily only after they were shifted upwards in energy to match the $9/2^+$ level to its experimental position. Furthermore, detailed inspection of the calculated wave functions indicated a fairly complex structure for all the states; a large fragmentation of the amplitudes was noted and contributions by a single orbital were found never to exceed 50% in any computed configuration. From a comparison of experimental and calculated branching ratios in the depopulation of three of the ^{67}Ni levels it was concluded that calculations with the JUN45 Hamiltonian gave consistently a somewhat better agreement. Clearly,

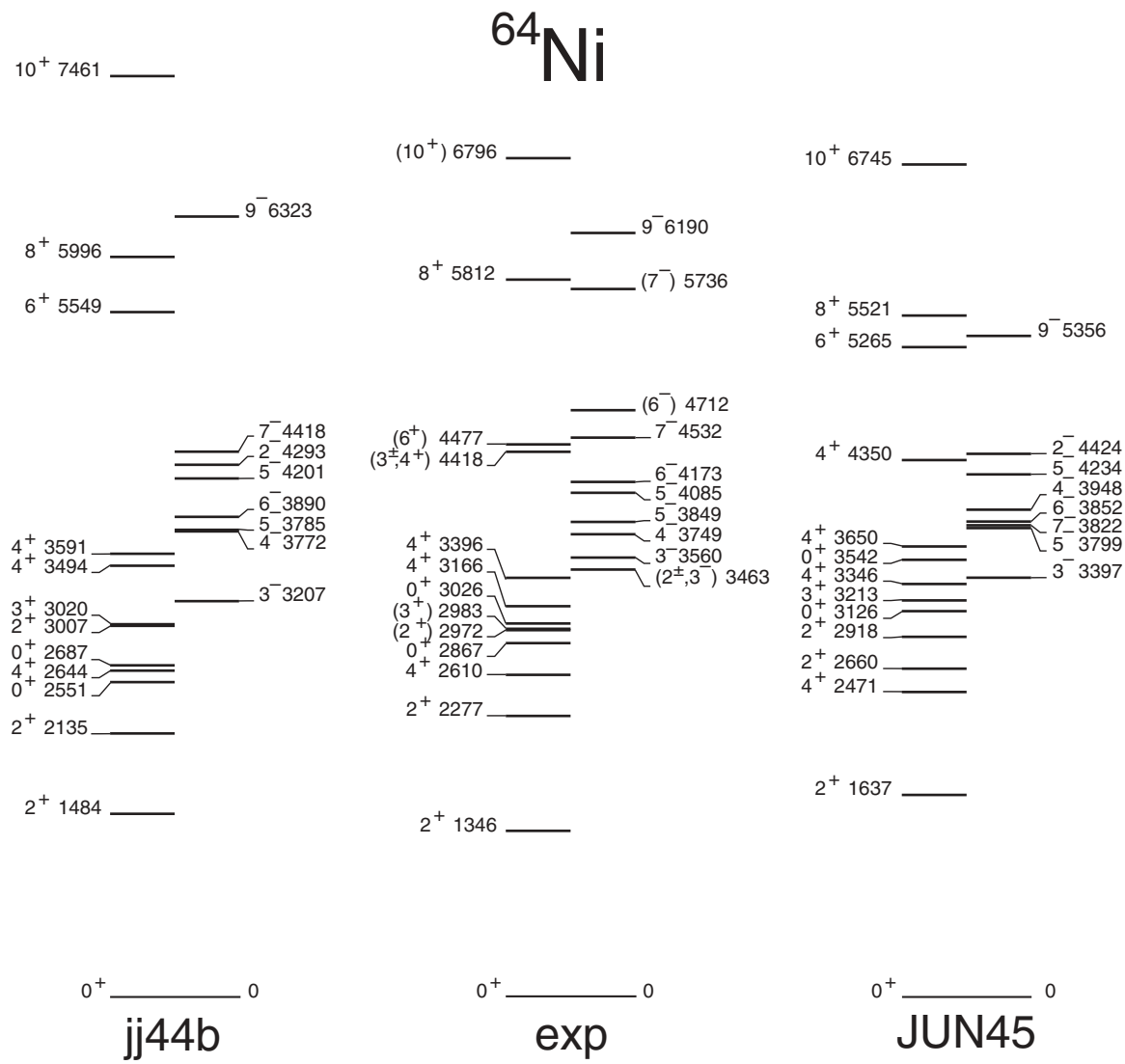

FIG. 13. Comparison of ^{64}Ni levels established in the experiment with two shell-model calculations. The jj44b (left) and JUN45 (right) labels denote results of calculations carried out with the two effective interactions discussed in the text. The negative- and positive-parity levels are displaced with respect to one another for the sake of clarity.

the situation remained unsatisfactory and in Ref. [18] the need for additional theoretical efforts aimed at improvement of the calculations was highlighted. The comparison of experimental and calculated levels in the even Ni isotopes discussed below should provide additional input to guide such improvements.

The results of calculations using both sets of interactions are compared with the ^{64}Ni, ^{66}Ni, and ^{68}Ni experimental levels in Figs. 13, 14, and 15, respectively. For transparency, the levels of different parity are separated and, in the calculated spectra, only the lowest energy levels for each spin with corresponding observed states are shown. Generally, the overall agreement between experiment and theory is rather satisfactory for all three isotopes and both sets of interactions.

In the case of ^{64}Ni, the jj44b calculations seem to reproduce the experimental levels better than the JUN45 ones, especially for negative-parity states: In this case, the excitation energies and the resulting yrast sequence match fairly well up to the highest level, with $I^{\pi} = 9^{-}$. Such an improvement is less clear when comparing globally experiment and theory for ^{66}Ni and ^{68}Ni, although the negative-parity states calculated with the JUN45 Hamiltonian appear to be systematically too low in energy for all three isotopes. This confirms the conclusion drawn in the ^{67}Ni study [18] (see above) that the adopted single-particle energy of the $g_{9/2}$ neutron orbital is too low in both Hamiltonians. In fact, it was found to be especially low for the JUN45 interaction with a calculated $9/2^{+}$ energy $\sim$0.5 MeV below the experimental value. Apparently, the consequence of too low a $g_{9/2}$ state energy is even magnified in the higher spin levels which require the involvement of two $g_{9/2}$ neutrons. For example, the 8^{+}, 10^{+}, and 12^{+} levels in ^{66}Ni are calculated by the JUN45 interaction to lay at energies

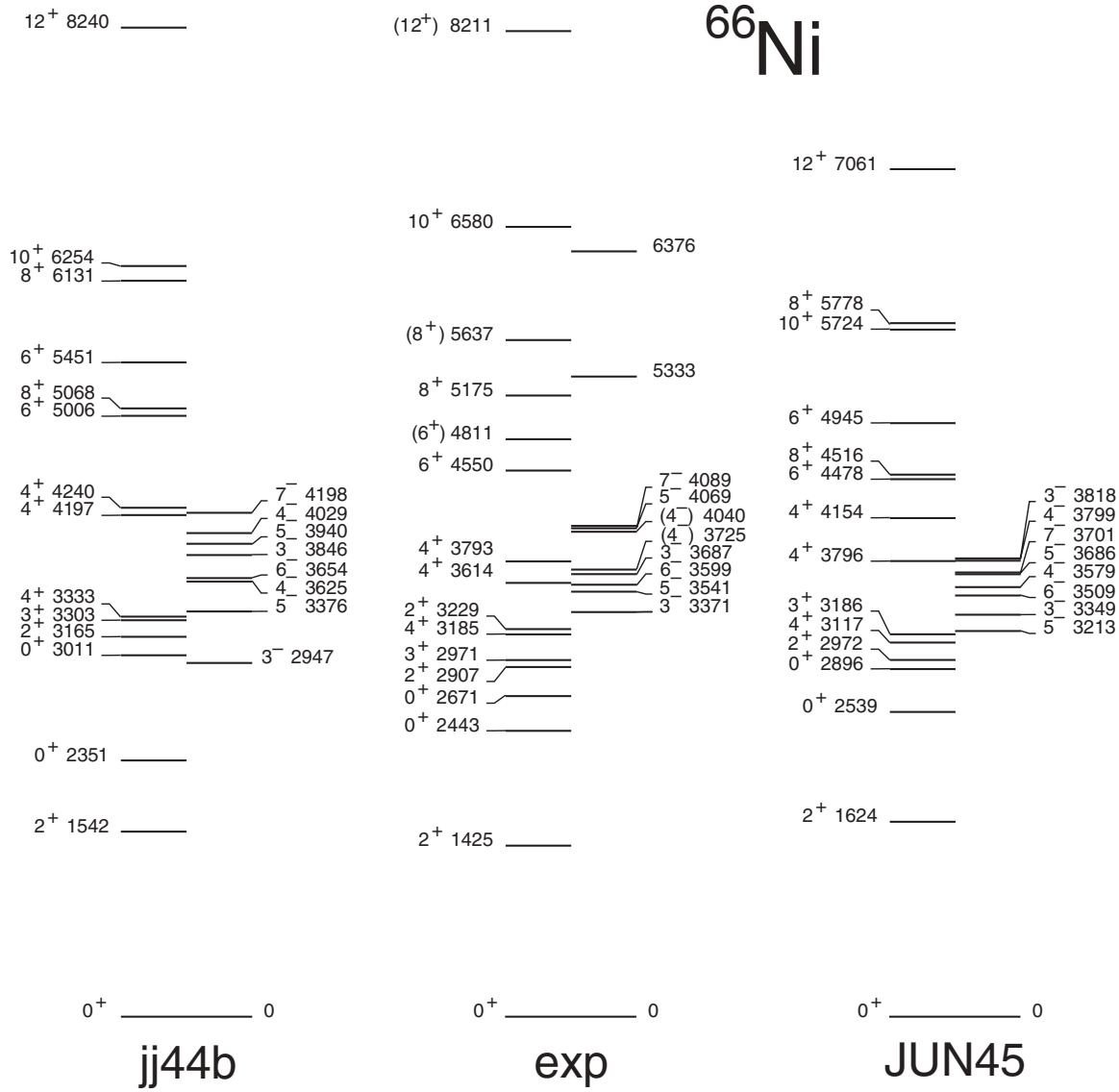

FIG. 14. Same as in Fig. 13, but for the ^{66}Ni isotope.

about 1 MeV below the actual data. However, it should also be recognized that the overall better agreement achieved with the jj44b calculations could be the consequence of the fact that the ^{64}Ni and ^{66}Ni experimental levels established earlier [19] were included in the fitting procedure.

For many ^{64}Ni, ^{66}Ni, and ^{68}Ni levels, the experimental energies match the calculated values to within 200 keV and the even better agreement observed in several instances is considered to be accidental. On the other hand, for some states the disagreement between experimental and calculated energies is much larger. Yet there does not appear to be any systematic trend that could provide useful guidance for future calculations.

Comparisons of the low-spin, positive-parity experimental levels in ^{64}Ni and ^{66}Ni with the calculations lead to the following observations. The two excited 0^+ states observed in both nuclei are calculated with energies reasonably close ($\sim$600 keV) to the experimental values. Here, the results with the JUN45 Hamiltonian appear to be in better agreement with experiment, reproducing both the energy separation between the excited 0^+ states and the shift to lower excitation energy occurring between ^{64}Ni and ^{66}Ni. However, the corresponding wave functions for both states are complex and do not readily provide insight into the origin of the much stronger population noted above (Sec. III B) for the higher-lying excited 0^+ state in ^{66}Ni following $2n$-transfer reactions and ^{66}Co β decay. On the other hand, the jj44b interaction reproduces better the experimental 2_1^+ and 2_2^+ states in both nuclei, especially the particularly low energy of the 2_2^+ level in ^{64}Ni, whereas the lowest 3^+ level in ^{66}Ni is calculated to lay more than 300 keV higher than the observed one. The computed energies of the yrast 4^+ states fit the data quite well, but much poorer agreement is observed for the second and third 4^+ levels, as well as for the 6^+ states which, especially in ^{66}Ni, are calculated by the jj44b interaction to lay at higher energies than experimentally observed. For example, no theoretical counterpart could be readily identified

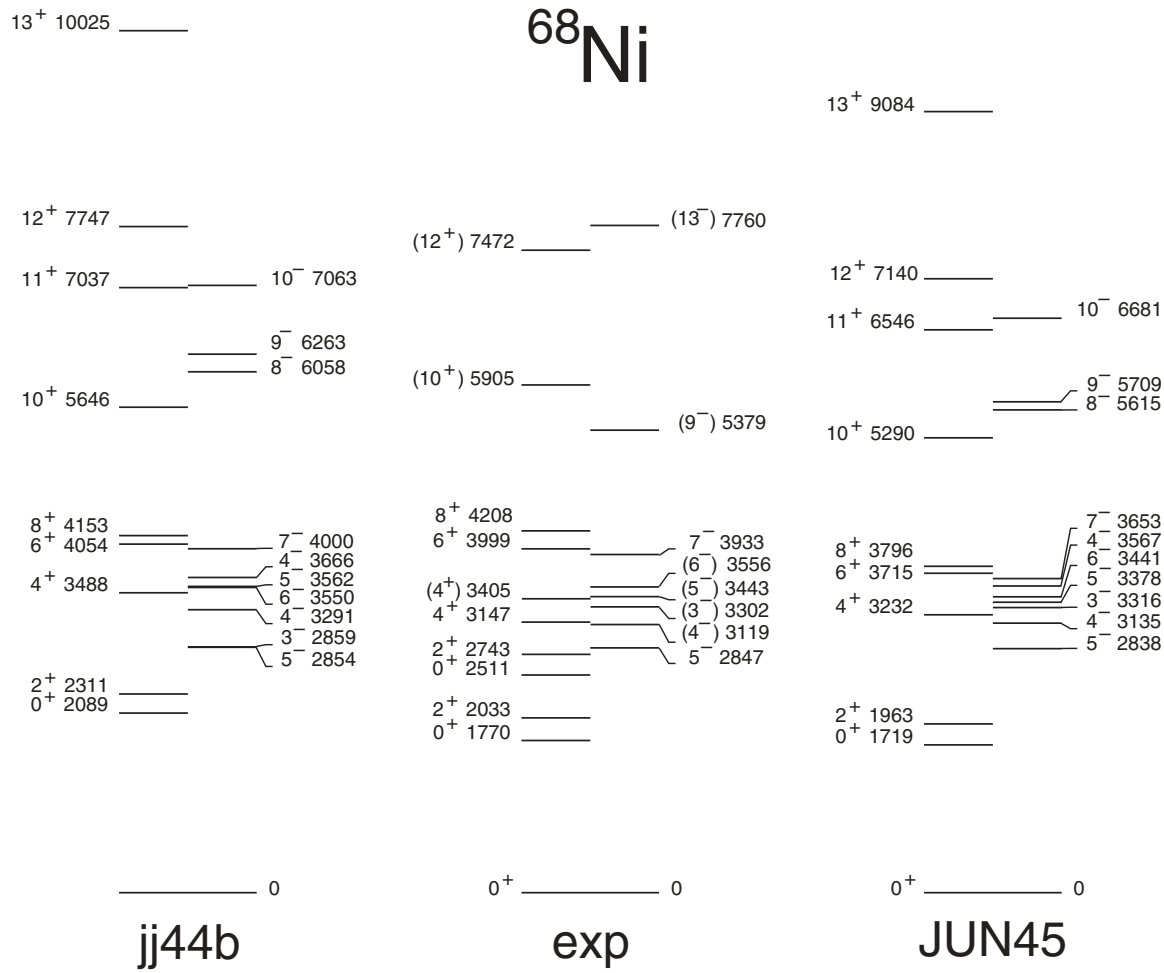

FIG. 15. Same as in Fig. 13, but for the ^{68}Ni isotope.

in ^{64}Ni for the tentatively assigned 6^+ state at 4477 keV, with the calculated 6^+_1 level located more than 1 MeV too high. Nevertheless, the overall agreement between theory and experiment is considered to be rather satisfactory, but in view of the apparent complexity of the level sequences and the accuracy of the calculations, it does not appear to be possible to provide an interpretation of every detail of the observed level structures.

To illustrate further some of the complexity noted above, the situation with the negative-parity states up to $I^\pi = 7^-$ is now considered in some detail. *A priori*, these levels should be characterized by intrinsic structures predominantly involving seniority-2 excitations with one neutron occupying the $p_{3/2}$, $f_{5/2}$, $p_{1/2}$ negative-parity orbitals and the other the $g_{9/2}$ single-particle state. In the data, the first 7^-, 6^-, and 5^- states are located at distinct yrast positions and capture the bulk of the γ-ray flow, which subsequently proceeds via fast *M1* transitions between them. This favored *M1* decay mode also selects the lower-spin, 4^- and 3^- states despite their unfavorable nonyrast status. The branching ratios observed for these *M1* decays reflect the complex microscopic structure of these negative-parity states as confirmed by the results of the calculations (see below). A strict quantitative comparison of the observed branching ratios with the calculations is made difficult by the significant mismatch between calculated and experimental level energies. Instead, one may try to understand the observations by examining the calculated wave functions in this series of negative-parity states, starting from the highest-spin 7^- level. In general, calculations with both the jj44b and JUN45 interactions indicate a similar, complex structure for these states, which involve typically more than ten configurations with a contribution to the wave functions exceeding 1%. Table V provides a simplified picture of these intrinsic structures calculated with both interactions. For each state, the computed energies are compared with the data and the main components of the wave functions other than the $g_{9/2}$ orbital are summarized in the last six columns in terms of the summed contributions (%) of all the amplitudes involving $f_{5/2}$, $p_{3/2}$, and $p_{1/2}$ unpaired neutrons. Apart from the observed similarity in the wave functions calculated with both interactions, it should be noted that, in general, the JUN45 results indicate a larger contribution from configurations with three or more $g_{9/2}$ neutrons than the jj44b ones. This appears to be a consequence of the low $g_{9/2}$ single-particle energy pointed

TABLE V. Summed contributions (%) of configurations involving unpaired $f_{5/2}$, $p_{3/2}$, and $p_{1/2}$ neutrons in wave functions calculated with the jj44b and JUN45 interactions for selected negative-parity states in ^{64}Ni, ^{66}Ni, and ^{68}Ni. The spin-parity assignments as well as experimental and calculated level energies are listed in the first four columns. See text for further details.

I^π	Level energy (keV) Exp.	Calc. jj44b	JUN45	jj44b (%)			JUN45 (%)		
				$f_{5/2}$	$p_{3/2}$	$p_{1/2}$	$f_{5/2}$	$p_{3/2}$	$p_{1/2}$
^{64}Ni									
7^-_1	4532	4418	3822	92	–	–	91	–	–
6^-_1	4173	3890	3852	66	12	6	86	6	3
5^-_1	3849	3785	3799	25	24	44	59	11	24
5^-_2	4085	4201	4234	38	31	21	34	28	30
4^-_1	3749	3772	3948	43	12	38	74	6	14
4^-_2	–	4284	4230	35	42	18	17	74	7
3^-_1	3560	3207	3397	13	75	3	10	84	2
(2^-_1)	3463	4293	4424	30	–	–	6	–	–
^{66}Ni									
7^-_1	4089	4198	3701	89	–	–	92	–	–
6^-_1	3599	3654	3509	75	9	8	87	4	3
5^-_1	3541	3376	3213	33	6	54	47	5	44
5^-_2	4069	3940	3686	59	10	23	49	5	41
(4^-_1)	3725	3625	3579	40	8	48	34	7	54
(4^-_2)	4040	4029	3799	60	20	12	53	13	29
3^-_1	3371	2947	3349	20	74	1	4	86	3
^{68}Ni									
7^-_1	3933	4000	3653	86	–	–	89	–	–
6^-_1	3556	3550	3441	82	8	–	87	5	–
5^-_1	2847	2854	2838	17	–				
78		14	3	78					
(5^-_2)	(3443)	3562	3378	74	5	16	77	5	14
(4^-_1)	(3119)	3291	3135	10	9	76	14	3	78
(3^-_1)	3302	2859	3316	26	65	5	8	88	1

out above. Using the simplified convention of Table V, the odd $g_{9/2}$ neutron will be omitted in the following discussion of the state structures, which focuses on the jj44b results. As expected, the highest-spin 7^- state in the ^{64}Ni, ^{66}Ni, and ^{68}Ni isotopes is of nearly pure $f_{5/2}$ character with 92%, 89%, and 86% respective contributions. Predominant $f_{5/2}$ contributions of 66%, 75%, and 82% are also calculated for the 6^-_1 levels. In contrast, the lower-spin states have a more complex composition with notably large $p_{3/2}$ and $p_{1/2}$ contributions varying in amplitude as the Fermi level moves across the orbitals of interest from ^{64}Ni to ^{68}Ni. In the three Ni isotopes, among the two 5^- states, the higher-lying 5^-_2 one is characterized by the larger $f_{5/2}$ component and, in ^{68}Ni, it constitutes again a predominant contribution of 74%. The higher-lying 4^-_2 state in ^{66}Ni involves a predominant $f_{5/2}$ contribution (60%) as well, whereas such a state was not observed in ^{64}Ni and ^{68}Ni. In all three isotopes, the $p_{1/2}$ orbital contributes substantially to the lowest 4^-_1 and 5^-_1 states and, in ^{68}Ni, such configurations dominate, amounting to 76% and 78% contributions, respectively. Whereas the more strongly bound $p_{3/2}$ single-particle orbital contributes to the wave functions of most of the negative-parity states under discussion, its largest amplitude is calculated for the 3^- levels, with essentially an equal contribution in both ^{64}Ni and ^{66}Ni, calculated as 75% and 85% with the jj44b and JUN45 interactions, respectively. The JUN45 energies for these 3^- levels are close to the experimental values, while the jj44b are too low by more than 300 keV. Hence, the situation is opposite to the more frequently encountered one, where the experimental 3^- state is shifted down in energy because of expected contributions from collective octupole excitations, which are not included in the shell-model calculations. Apparently, this type of collectivity is practically absent in these Ni isotopes and the dominant $p_{3/2}{}^{-1}g_{9/2}$, *E3* neutron excitation is not able to drive the required high-energy *E3* proton ones. Finally, a rather unclear situation occurs with the 3463-keV state in ^{64}Ni, which was tentatively assigned as $I^\pi = (2^\pm,3^-)$, but with a preference for the 2^- assignment based on results from the neutron capture reaction of Ref. [29] and from ^{64}Co β decay [27] (see Sec. III A). The 2^- state is *a priori* expected to arise predominantly from the $f_{5/2}$ $g_{9/2}$ coupling and any other amplitude must involve higher-seniority excitations. However, the calculated $f_{5/2}$ contributions to the state wave function are only 30% and 6% in the two Hamiltonians while the computed

energies are off by 0.8 and 1.0 MeV, respectively. Alternative 2^+ or 3^- assignments to the 3463-keV level would require an explanation for several puzzling experimental features observed in the present study and in other investigations as discussed in Sec. III A.

The wave functions of the negative-parity states (Table V) can account to some extent for the dominance of interconnecting *M1* transitions and the fairly rare occurrence of competing *E2* decay branches. The difference in the g-factor values between the $g_{9/2}$ and any of the coupled $p_{3/2}$, $f_{5/2}$, or $p_{1/2}$ neutrons are sufficiently large to result in sizeable *M1* decay strengths between $\Delta I = 0,1$ states involving these components of the wave functions. On the other hand, among all the *M1* transitions requiring the change of the $p_{3/2}$, $f_{5/2}$, or $p_{1/2}$ components alone, only the $p_{3/2} \rightarrow p_{1/2}$ spin-flip change will result in fast *M1* transitions. However, it should be recognized that these arguments of a general nature do not explain the selectivity noted in the data for some of the *M1* decays, as is discussed below.

In ^{64}Ni, the two 5^- levels are characterized by fairly similar structures (see Table V), yet the *M1* decay from the 6^- state populates only the 5^-_1 level and the expected *M1* branch to the 5^-_2 state is not observed even though it would be expected to have an intensity of 0.4 units in Table I. Perhaps even more surprising are the deexcitation modes from this 5^-_2 level where the $5^-_2 \rightarrow 5^-_1$ branch competes with the retarded *E1* transitions of higher energy to the two 4^+_1 and 4^+_2 states, while the energy-favored $5^-_2 \rightarrow 4^-$ *M1* decay was not observed.

In ^{66}Ni, apart from noting the $7^-_1 \rightarrow 6^-_1 \rightarrow 5^-_1$ sequence of strong *M1* transitions in line with the general expectations above, it is worth considering the two 5^- and 4^- states. The decay of the 5^-_1 level was already discussed in Sec. III B. The presence of sizable $p_{1/2}$ and $f_{5/2}$ contributions to the calculated wave functions of the 5^-_1 and 3^-_1 states may be invoked to explain the observed 171-keV *E2* decay branch in competition with the retarded 356-keV *E1* deexcitation. The 5^-_2 level deexcites to the available negative-parity states through five γ branches, of which three are of *M1* character. The relative reduced transition probabilities measured for the 345-keV ($5^-_2 \rightarrow 4^-_1$) and 529-keV ($5^-_2 \rightarrow 5^-_1$) transitions are similar in strength, but the 470-keV *M1* $5^-_2 \rightarrow 6^-_1$ branch is five times faster. Also the 4^-_1 state is deexcited via two *M1* transitions of comparable strengths to the 5^-_1 and 3^-_1 levels, while the 4^+_2 state populates the 3^-_1 level selectively with possible branches to the 4^-_1 and 5^-_1 levels remaining below the detection limit.

While a quantitative understanding of every *M1* decay in both ^{64}Ni and ^{66}Ni seems to be beyond the reach of the present calculations, the situation appears to be simpler in the case of ^{68}Ni. Here, the calculated wave functions indicate less complex structures than for the two lighter isotopes. Also, the agreement between measured and calculated levels (see Fig. 15) is the closest for both the jj44b and the JUN45 interactions. Starting from the 8^+ $\nu(g_{9/2})^2$ isomeric state (see Fig. 12) the decay proceeds partly through a cascade of four *E2* transitions toward the ground state, but 2/3 of the intensity proceeds through the sequence of negative-parity levels ending into the 5^-_1 long-lived state. Although among these states only the 7^- level was assigned firm spin and parity values in the work of Ref. [6], the assignments of 6^-_1, 5^-_2, and 4^-_1 to the lower members of the sequence is strongly preferred by the observed γ decays as well as by the results of the shell-model calculations. The wave functions listed in Table V indicate a predominant $\nu(f_{5/2}g_{9/2})$ structure for the 7^-_1, 6^-_1, and 5^-_2 states and a main $\nu(p_{1/2}g_{9/2})$ configuration for the 4^-_1 and 5^-_1 levels. The observed decay pattern is fully consistent with this interpretation: The 1086-keV transition discovered in this work represents the $f_{5/2} \rightarrow p_{1/2}$ *E2* decay, which is able to compete with the strong *M1* transition to the 6^-_1 level. Based on the measured intensities, the 113-keV *M1* transition depopulating the 6^-_1 state to the 5^-_2 level is 140 times faster than the 709-keV *M1* decay to the 5^-_1 state. However, the 324- and 596-keV *M1* decays from the 5^-_2 level toward, respectively, the 4^-_1 and 5^-_1 states that involved strikingly different configurations are more comparable with one another and the 324-keV decay is only 6 times faster than the 596-keV transition.

For the highest-spin levels in ^{68}Ni, the suggested spin-parity assignments should be considered as very tentative, although the calculations with both interactions compute 9^-, 10^+, and 12^+ levels close to the experimental ones. The low energy of 287 keV for the transition feeding selectively the presumed 12^+ state is in line with the suggested 13^- assignment to the highest state seen in the present work at 7760 keV. This level may possibly correspond to the highest-spin, seniority-4 state with the $(g_{9/2})^3 f_{5/2}$ configuration which is expected in this energy range even though it was not computed in the present calculations.

Finally, the recently identified low-spin states, discussed in the last part of Sec. III C, can also be interpreted within the framework of the shell model. For the 3^- states in ^{64}Ni and ^{66}Ni, a particularly good agreement between calculated and experimental level energies was obtained with the JUN45 interaction. In ^{68}Ni, the tentatively assigned 3^- state at 3302 keV was calculated with this interaction to lay at 3316 keV, very close in energy to the data. As in lighter isotopes, the $\nu(p_{3/2}g_{9/2})$ configuration contributes predominantly to the configuration associated with this level (see Table V). Although a second excited 4^+ state was not calculated, based on the arguments below, one should expect to find two close-lying 4^+ states such as the 3147- and 3405-keV levels observed in the experiment. While the firmly assigned 3147-keV, 4^+_1 level, strongly populated in the *E2*-decay sequence from the $\nu(g_{9/2})^2$ 8^+ isomer, must be dominated by the $\nu(g_{9/2})^2{}_{4+}$ configuration, the character of the 3405-keV state, suggested as the 4^+_2 level, might be similar to that of the 4^+_1 state in ^{66}Ni, which has a predominant contribution of the $(g_{9/2})^2_{0+}$ neutron pair. The absence of a competing *E2* branch from the 3999-keV, 6^+ level to this 4^+_2 state and its decay selecting the 2^+_2 level rather than 2^+_1 state indicates the structural difference between both 4^+ states. These observations may also shed light on the different structures associated with two lowest 2^+ states in ^{68}Ni.

V. CONCLUSIONS

Excited states in the neutron-rich ^{64}Ni, ^{66}Ni, and ^{68}Ni isotopes, produced in 430-MeV $^{64}\mathrm{Ni} + {}^{238}\mathrm{U}$ collisions, were studied with γ-spectroscopy coincidence techniques. The

information available prior to this work was significantly expanded and now includes many nonyrast states populated with intensities down to 0.2%–0.4% of the channel of interest. Spin-parity assignments were proposed based on an angular-correlation analysis whenever sufficient statistics was available. Apart from assignments to newly established levels, a number of such I^π values suggested in earlier work were verified or sometimes corrected. The procedure often involved also a critical review of information available from all previous studies. The γ-ray cross-coincidence technique was used to enhance the population of nonyrast states through selection of quasielastic reactions. The method also provided a means to confirm spin values. Using the delayed-coincidence analysis technique, the previously established isomeric states in ^{66}Ni and ^{68}Ni were confirmed, information on their various deexcitation pathways was significantly expanded, and states located above these long-lived levels were established. In ^{68}Ni, the population of recently identified low-spin states [37] was confirmed as well.

Shell-model calculations were carried out with two modern effective interactions, JUN45 and jj44b, for the $p_{3/2}f_{5/2}p_{1/2}g_{9/2}$ space, using ^{56}Ni as a core. Satisfactory agreement between experiment and theory was achieved. However, in the case of ^{64}Ni and ^{66}Ni, a detailed understanding of the level structure is not yet provided by the present calculations as the wave functions involve admixtures of a large number of configurations. This apparent complexity was illustrated by considering the structure of the negative-parity states and the characteristics of the *M1* transitions linking them. The best agreement between experiment and theory was achieved for ^{68}Ni, where the calculations also associate the simplest configurations with the observed states.

In the present study, no evidence was found for collective motion that could potentially affect shell-model descriptions. Although the general picture, with states characterized by configurations with many single-particle components, is rather complex, improvements of shell-model descriptions remain highly desirable. For example, the role of neutron orbitals other than the $g_{9/2}$ state above the $N = 40$ subshell gap should be explored to progress in understanding the neutron degrees of freedom in these Ni isotopes characterized by a largely intact closed $Z = 28$ proton shell. Efforts in this direction are under way. For example, an interaction involving the $d_{5/2}$ orbital in addition to the $g_{9/2}$ state has recently been proposed [47], but has not yet been applied to the Ni isotopes.

It is hoped that the experimental level schemes established in the present work will stimulate further theoretical efforts. Interesting structural changes taking place in nuclei with proton numbers departing from the $Z = 28$ shell closure might then be understood better and this, in turn, might stimulate a quest for such changes at higher spins and excitation energies in the Ni isotopes themselves. The latter experimental challenge in the study of the Ni isotopes will likely require the use of radioactive beams.

ACKNOWLEDGMENTS

The authors thank the ATLAS operating staff for the efficient running of the accelerator and J. P. Greene for target preparations. This work was supported by the US Department of Energy, Office of Nuclear Physics, under Contract No. DE-AC02-06CH11357 (A.N.L.) and Grant No. DE-FG02-94ER40834 (U.M.), and by the Polish National Science Center, Project No. NN202-008640.

[1] O. Sorlin and M.-G. Porquet, Prog. Part. Nucl. Phys. **61**, 602 (2008).
[2] R. V. F. Janssens, Nature (London) **459**, 1069 (2009).
[3] M. Bernas, Ph. Dessagne, M. Langevin, J. Payet, F. Pougheon, and P. Roussel, Phys. Lett. B **113**, 279 (1982).
[4] R. Broda *et al.*, Phys. Rev. Lett. **74**, 868 (1995).
[5] R. Grzywacz *et al.*, Phys. Rev. Lett. **81**, 766 (1998).
[6] T. Ishii, M. Asai, A. Makishima, I. Hossain, M. Ogawa, J. Hasegawa, M. Matsuda, and S. Ichikawa, Phys. Rev. Lett. **84**, 39 (2000).
[7] R. Broda *et al.*, *Proceedings of the International Conference on Fission and Properties of Neutron-Rich Nuclei, Sanibel Island, Florida 1997*, edited by J. H. Hamilton and A. V. Ramayya (World Scientific Publ. Co., Singapore, 1998), pp. 202–213.
[8] T. Ishii *et al.*, Phys. Rev. Lett. **81**, 4100 (1998).
[9] I. Stefanescu *et al.*, Phys. Rev. C **79**, 034319 (2009).
[10] M. Hannawald *et al.*, Phys. Rev. Lett. **82**, 1391 (1999).
[11] W. F. Mueller *et al.*, Phys. Rev. Lett. **83**, 3613 (1999).
[12] O. Sorlin *et al.*, Eur. Phys. J. A **16**, 55 (2003).
[13] L. Gaudefroy *et al.*, Eur. Phys. J. A **23**, 41 (2005).
[14] P. Adrich *et al.*, Phys. Rev. C **77**, 054306 (2008).
[15] A. Gade *et al.*, Phys. Rev. C **81**, 051304(R) (2010).
[16] J. Ljungvall *et al.*, Phys. Rev. C **81**, 061301(R) (2010).
[17] W. Rother *et al.*, Phys. Rev. Lett. **106**, 022502 (2011).
[18] S. Zhu *et al.*, Phys. Rev. C **85**, 034336 (2012).
[19] T. Pawłat *et al.*, Nucl. Phys. A **574**, 623 (1994).
[20] R. Broda, J. Phys. G: Nucl. Part. Phys. **32**, R151 (2006).
[21] C. J. Chiara *et al.*, Phys. Rev. C **82**, 054313 (2010).
[22] N. Hoteling *et al.*, Phys. Rev. C **82**, 044305 (2010).
[23] C. J. Chiara *et al.*, Phys. Rev. C **85**, 024309 (2012).
[24] Balraj Singh, Nucl. Data Sheets **108**, 197 (2007).
[25] E. Browne and J. K. Tuli, Nucl. Data Sheets **111**, 1093 (2010).
[26] I.-Y. Lee, Nucl. Phys. A **520**, 641c (1990).
[27] D. Pauwels *et al.* [Phys. Rev. C (to be published)].
[28] P. E. Haustein, Nucl. Instrum. Methods **99**, 433 (1972).
[29] A. Harder, S. Michaelsen, A. Jungclaus, K. P. Lieb, A. P. Williams, H. G. Borner, and M. Trautmannsheimer, Z. Phys. A **343**, 7 (1992).
[30] W. Darcey, R. Chapman, and S. Hinds, Nucl. Phys. A **170**, 253 (1971).
[31] W. P. Alford, R. N. Boyd, E. Sugarbaker, D. L. Hanson, and E. R. Flynn, Phys. Rev. C **21**, 1203 (1980).
[32] U. Bosch *et al.*, Nucl. Phys. A **477**, 89 (1988).
[33] W. F. Mueller *et al.*, Phys. Rev. C **61**, 054308 (2000).
[34] E. A. McCutchan, Nucl. Data Sheets **113**, 1735 (2012).
[35] S. N. Liddick *et al.*, Phys. Rev. C **85**, 014328 (2012).
[36] A. Dijon *et al.*, Phys. Rev. C **85**, 031301(R) (2012).
[37] C. J. Chiara *et al.*, Phys. Rev. C **86**, 041304 (2012).

[38] M. R. Bhat, Nucl. Data Sheets **85**, 415 (1998).
[39] C. M. Baglin, Nucl. Data Sheets **95**, 215 (2002).
[40] M. R. Bhat, Nucl. Data Sheets **88**, 417 (1999).
[41] B. Erjun and H. Junde, Nucl. Data Sheets **92**, 147 (2001).
[42] E. Browne and J. K. Tuli, Nucl. Data Sheets **111**, 2425 (2010).
[43] E. Caurier and F. Nowacki, Acta Phys. Pol. B **30**, 705 (1999).
[44] E. Caurier, shell-model code ANTOINE (IRES, Strasbourg, 1989–2004).
[45] M. Honma, T. Otsuka, T. Mizusaki, and M. Hjorth-Jensen, Phys. Rev. C **80**, 064323 (2009).
[46] B. A. Brown (private communication); see also Ref. [28] in B. Cheal *et al.*, Phys. Rev. Lett. **104**, 252502 (2010).
[47] S. M. Lenzi, F. Nowacki, A. Poves, and K. Sieja, Phys. Rev. C **82**, 054301 (2010).